





**JEVGENI ŠULGA**

Self-assembly and  
interaction of nanostructures



TARTU UNIVERSITY PRESS

Institute of Physics, Faculty of Science and Technology, University of Tartu,  
Estonia

Dissertation in Material Science

The dissertation was admitted on 23.11.2011 in partial fulfillment of the requirements for the degree of Doctor of Philosophy in material science, and allowed for defense by the Scientific Council on Material Science of the Faculty of Science and Technology of the University of Tartu.

Supervisor: Dr. Ilmar Kink, Institute of Physics, University of Tartu,  
Estonian Nanotechnology Competence Centre

Opponents: Dr. Albert Nasibulin, Docent, Department of Applied Physics,  
Aalto University School of Science

Dr. Renno Veinthal, Professor, Department of Materials  
Engineering Faculty of Mechanical Engineering,  
Tallinn University of Technology

Commencement 27.01.2012 at the University of Tartu, Tartu, Estonia

This work has been supported by graduate school School on “Functional Materials and Technologies” (GSFMT), University of Tartu and Tallinn University of Technology, EU Social Funds project 1.2.0401.09-0079



European Union  
European Social Fund



Investing in your future

ISSN 2228–0928

ISBN 978–9949–19–927–3 (trükis)

ISBN 978–9949–19–928–0 (PDF)

Autoriõigus: Jevgeni Šulga, 2011

Tartu Ülikooli kirjastus

[www.tyk.ee](http://www.tyk.ee)

Tellimus nr. 806

# CONTENTS

CONTENTS.....	5
LIST OF ORIGINAL PUBLICATIONS.....	7
AUTHOR's CONTRIBUTIONS.....	8
LIST OF USED ABBREVIATIONS .....	9
1. PREFACE.....	10
2. CARBON NANOTUBES.....	11
2.1. Structures of Carbon Materials .....	11
2.2. Structures of Carbon Nanotubes .....	12
2.3 Nitrogen containing CNT .....	15
3. CARBON NANOTUBES: METHODS OF PRODUCTION.....	18
3.1. Arc discharge .....	18
3.2. Laser Ablation Technique.....	18
3.3. Chemical Vapor Deposition.....	19
3.4. Hot wall CVD reactor .....	19
3.5. Cold-wall CVD reactor.....	20
4. CARBON NANOTUBE GROWTH MECHANISM DURING CVD .....	21
4.1. Synthesis of nitrogen-containing nanotubes .....	22
5. FUNCTIONALIZATION OF CARBON NANOTUBES .....	24
5.1. Interests and types of functionalization .....	24
5.2. Non-covalent functionalization with surfactants or polymers .....	25
5.3. Covalent Functionalization of Carbon Nanotubes .....	26
6. CHARACTERIZATION METHODS.....	30
6.1. Scanning Electron Microscopy .....	30
6.2. Fundamental principles.....	30
6.3. Energy Dispersive Spectroscopy .....	32
6.4. X-Ray Photoelectron Spectroscopy (XPS) .....	33
7. SYNTHESIS OF MILLIMETER SCALE ALIGNED CARBON NANOTUBES: EXPERIMENTAL RESULTS (Paper – V).....	34
7.1. Preparation of Catalyst Layers.....	34
7.2. Experimental setup and synthesis parameters.....	36
8. SYNTHESIS OF CNT AND NITROGEN DOPED CARBON NANOTUBES ON GLASSY CARBON ELECTRODES: EXPERIMENTAL RESULTS (Paper – I).....	38
8.1. Experimental setup.....	38
8.2. Preparation of catalyst materials .....	39
8.3. Synthesis of CNT and nitrogen doped CNT on Glassy Carbon electrodes .....	40

8.4. Characterisation of NCNT .....	42
9. GAS PHASE FUNCTIONALIZATION OF ALIGNED CNT WITH NITRIC ACID VAPOR (Paper – V) .....	44
9.1. Experimental setup.....	44
9.2. Results and Discussion. ....	45
10. FORMATION OF NICKEL OXIDE NANOSTRUCTURES ON TiO <sub>2</sub> (Paper – II).....	51
11. PREPARATION OF STRUCTURED SOL-GEL FILMS USING TAPE CASTING METHOD (Paper – III) .....	53
12. METHOD OF CLEANING THE TIP OF ATOMIC FORCE MICROSCOPY (Patent IV).....	56
SUMMARY AND CONCLUSION .....	58
SUMMARY IN ESTONIAN.....	59
REFERENCES .....	60
ACKNOWLEDGEMENTS.....	64
PUBLICATIONS.....	65

## LIST OF ORIGINAL PUBLICATIONS

- I. Alexeyeva N., Shulga E., Kisand V., Kink I., Tammeveski K. Electro-reduction of oxygen on nitrogen-doped carbon nanotube modified glassy carbon electrodes in acid and alkaline solutions. *Journal of Electro-analytical Chemistry*, 2010, 648, 169–175
- II. Shulga J., Kisand V., Kink I., Reedo V., Matisen L., Saar A. Formation of nickel oxide nanostructures on TiO<sub>2</sub>. *Journal of Physics: Conference Series*, 2007, 93, 1–6
- III. Kisand V., Shulga J., Tätte T., Visk U., Natali M., Mistura G., Paalo M., Lobjakas M., Kink I. Preparation of structured sol-gel films using tape casting method. *Materials Science and Engineering B-Solid State Materials for Advanced Technology*, 2007, 137, 162–165
- IV. Vlassov S., Lõhmus A., Lõhmus R., Kink I., Šulga J. Method for cleaning the atomic force microscope tip and the sample. Patented invention, priority number: P200700031; priority date: 12.06.2007. Owners: Estonian Nanotechnology Competence Centre, University of Tartu
- V. Shulga E., Pohako K., Treshchalov A., Joost U., Kisand V., Kink I. Functionalization of aligned carbon nanotubes with nitric acid vapor. *Micro and Nano Letters*, 2011, 6, 704–708

## **AUTHOR's CONTRIBUTIONS**

Paper I: the author participated in development of experimental equipment, in experiments and data processing, and is responsible for composing experimental part of the manuscript.

Paper II: the author is responsible for measurements of the thin films with Atomic Force Microscope, and wrote description of the measurements in manuscript.

Paper III: the author is responsible for synthesis of the catalyst layer, and development of chemical vapor deposition reactor for synthesis of nitrogen doped carbon nanotubes. The author also synthesized nitrogen doped carbon nanotubes and composed experimental part of the manuscript.

Patent IV: the author is responsible for Atomic Force Microscope measurements, and processing of the images.

Paper V: the author is responsible for the main idea of the work, and for development of the reactor. The author also participated in synthesis of millimeter scale carbon nanotubes and functionalization experiments. He did measurements with electron microscope and elemental analysis, and composed the manuscript.



## **LIST OF USED ABBREVIATIONS**

SWCN	–	Single-walled carbon nanotube
MWCN	–	Multi-walled nanotube
CNT	–	Carbon nanotube
CNF	–	Carbon nano fiber
NCNT	–	Nitrogen containing CNT
CVD	–	Chemical vapor deposition
PECVD	–	Plasma enhanced chemical vapor deposition
BSE	–	Backscattered electrons
SEM	–	Scanning electron microscope
EDS	–	Energy dispersive spectroscopy
XPS	–	X-Ray Photoelectron Spectroscopy
ACNT	–	Aligned carbon nanotubes
GC	–	Glassy carbon
AFM	–	Atomic Force Microscopy

# I. PREFACE

Applications of nanotechnology are considered among the key elements in technological development. Despite massive effort the new technologies have not submerged into economy rapidly enough and further research to improve the technologies is clearly needed.

The current research is a part of a larger combined effort towards development of a platform of new complex and functional materials and micro- and nanostructures based on carbon nanostructures. Implementation and development of new methods for growing CNT is certainly a critical step towards the goal.

The thesis is related to several important issues in the research field – catalyst particles and substrate preparation for CNT synthesis, synthesis of CNT and NCNT, functionalization of CNT in gas phase, and thus can be considered as multidisciplinary. However, all of these topics focus on preparation of nanostructured materials from “bottom up”, i.e. preparation of structures from smaller building blocks, and can thus be considered as self-assembled structures (nanoparticles formation, CNT alignment, etc.).

The thesis begins from theoretical background explaining what are CNTs, about their synthesis, functionalization and most used characterization methods. In preparation of theoretical section the following works were used: [1], [9], [10], [12], [13], [35], [39], [44], [90], [94].

The main part of the experimental section of the thesis is dedicated to synthesis of ACNT, NCNT and gas-phase functionalization possibilities of such structures. Following sections describe original sol-gel prepared catalyst material and possibility of its microstructuring. Also, a new patented method for cleaning atomic force microscope tip is described.

The work was performed mainly at the Institute of Physics, University of Tartu.

## 2. CARBON NANOTUBES

First evidence for the tubular nature of nano-sized carbon filaments was published in 1952 [2] and many other reports have followed over the next forty years [3], [4], [5]. However, these fibers were not recognized as nanotubes and were not studied systematically. It was only after the discovery of fullerenes in 1985 [6] that carbon nanostructures were explored further and attracted global scientific attention. Interest in CNT research began in 1991 from publication of the Japanese electron microscopist Sumio Iijima [7]. In 1993 two distinctive research groups demonstrated independently the ability to produce single-sheet tubules, coiled as SWNTs and observed tubular features in carbon soot produced in an arc discharge. The structure of these tubules composed of concentric multiwalls forming one cylinder defining a MWNT [8],[9]. Promising physical, chemical and electronic properties of CNTs have been highlighted in the next years, leading to a great expansion of the breadth and range of research dedicated to these nanoparticles over the past several years. Once considered a novelty, CNT are today a key foundational material of the nanotechnology.

### 2.1. Structures of Carbon Materials

Carbon can exist in many forms varying its chemical and physical properties that will be detailed in later sections. Carbon atoms have six electrons, occupying the  $1s^2$ ,  $2s^2$ , and  $2p^2$  orbitals. The bond strength between the valence electrons in the outer two orbitals is weaker than that in the  $1s^2$  orbital, thus allowing a mixing or hybridization of the electrons. This mixing is made possible by the small energy difference between the  $2s$  and  $2p$  energy levels and three hybridization states are possible:  $sp$ ,  $sp^2$  and  $sp^3$ . Table 1, compiled by Saito et al. [10], shows some of the physical parameters given for the isomers made possible by the different hybridizations of carbon.

**Table 1.** Some parameters given for the isomers made possible by the different hybridizations of carbon [10].

Dimension	0-D	1-D	2-D	3-D
	$C_{60}$	Carbon nanotube	Graphite	Diamond
hybridization	$sp^2$	$sp^2$	$sp^2$ (sp)	$sp^3$
Density ( $g/cm^3$ )	1.72	1.2–2.0	2.26	3.515
Bond Length ( $\text{\AA}$ )	1.4	1.44	1.42	1.54
Electronic properties	Semiconductor $E_g = 1.9 \text{ eV}$	Metal or Semiconductor	Semi-Metal	Insulator $E_g = 5.47 \text{ eV}$

In the  $sp^3$  hybridisation the 2s orbital hybridises with all three 2p orbitals and form four equivalent  $sp^3$  orbitals arranged tetrahedrally around the nucleus (Figure 1). A simple example for a  $sp^3$  hybridization provide the carbon atoms in ethane ( $C_2H_6$ ). If the 2s orbitals hybridise with two of the 2p orbitals three  $sp^2$  orbitals are formed and one unhybridised 2p orbital is left. The  $sp^2$  orbitals are in a plane oriented at  $120^\circ$  to each other and can form  $\sigma$  bonds by overlapping with  $sp^2$  orbitals of neighbouring atoms as seen in  $C_2H_4$  (ethylene). The remaining p orbitals on both C atoms perpendicularly oriented to the plane form a  $\pi$  bond by overlapping with the corresponding orbitals of the neighbouring C atoms ( $C=C$ ). In the  $sp$  hybridisation a linear combination of the 2s orbital with one of the 2p orbital is formed. Two  $sp$  hybridised carbon atoms are bonded by overlapping their  $sp$  orbitals ( $\sigma$  bond). The remaining two p orbitals of each carbon atom form a  $\pi$  bond. This hybridisation can be seen in acetylene ( $C_2H_2$ ) and is represented by  $C\equiv C$ .

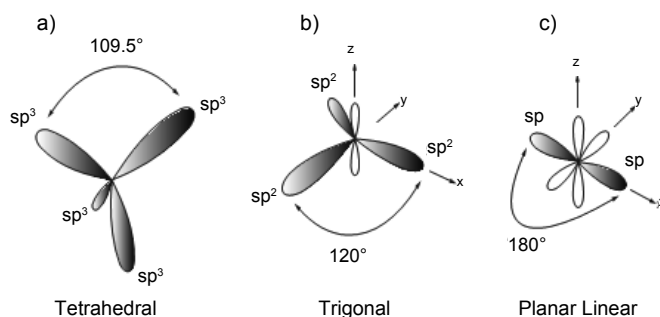


**Figure 1.** The 3 different hybridisation states of carbon a)  $sp^3$ , b)  $sp^2$ , c)  $sp$  [11].

## 2.2. Structures of Carbon Nanotubes

The hybridization configuration  $sp^2$  is not only able to form a planar structure as occurring in graphite. The graphene sheet can also be wrapped up into a closed polyhedra (0-dimensional) e.g. as in fullerenes or rolled up into cylinders (1-dimensional) as in CNTs. CNTs can be divided into following structures (Figure 2): fishbone type CNF (a), SCNT (b), MCNT (c) and bamboo structured CNT (d).

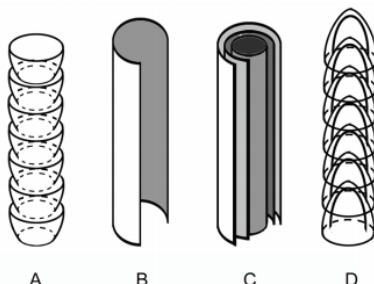


**Figure 2.** Structure of a) CNF b) SWNT c) MWNT and d) bamboo CNT [12].

The structure of an individual CNT can be specified in terms of a vector, the chiral vector  $C_h$  that joins two crystallographically equivalent sites on the original graphene sheet [13]. When this hexagonal lattice is rolled up (Figure 3), the two end-points of the vector are superposed to form the cylinder. The vector  $C_h$  can be described by the following relation:

$$C_h = na_1 + ma_2 \quad (I),$$

where  $a_1$  and  $a_2$  are unit vectors of the hexagonal lattice and  $n$  and  $m$  are translational indices. Each nanotube topology is usually characterized by these two integer numbers ( $n,m$ ) leading to a primary symmetry classification of nanotubes. A chiral nanotube is defined by a nanotube whose mirror image cannot be superposed to the original one. On the contrary, the structure of an achiral nanotube is undistinguishable from the mirror image one.

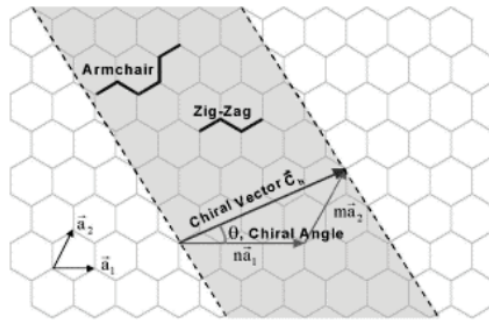


**Figure 3.** Schematic diagram showing how a hexagonal sheet of graphite is ‘rolled’ to form a CNT [14]

There are only two cases of achiral nanotubes: armchair ( $n,n$ ) and zig-zag ( $n,0$ ) nanotubes (Figure 4). The nanotube structure can be also defined by the chiral angle  $\theta$  between the vectors  $C_h$  and  $a_1$ , with values of  $\theta$  in the range  $0^\circ$ – $30^\circ$  due to the hexagonal symmetry of the lattice. The two limit cases correspond to achiral nanotubes with values of  $0^\circ$  and  $30^\circ$  respectively for zig-zag and armchair classes.

In the MWCNTs (Russian doll model), each individual concentric tube can have different chirality. This primary symmetric classification of CNTs is very important because variations in the nanotube morphology can lead to changes in the properties of the nanotube. For example, the structure of a CNT determines its electronic behaviour. Indeed, the electronic properties of a nanotube follow a general rule: if  $(n-m)$  is a multiple of 3, then the tube exhibits a metallic behaviour, otherwise it is an electrical semiconductor [15]. Investigations of the influence of chirality on the mechanical properties of CNTs have also been reported. So, armchair nanotubes present a metallic behaviour while zig-zag

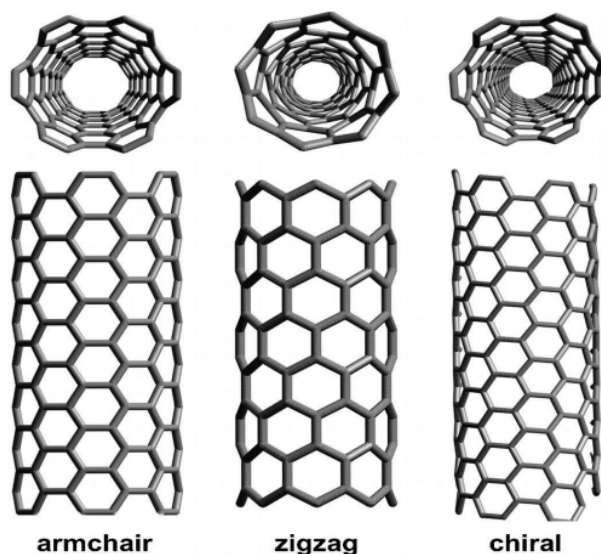


**Figure 4.** Illustrations of the atomic structure of armchair, zig-zag and chiral nanotubes [16].

and chiral nanotubes can be either metallic or semiconducting [17]. Although the chirality has a relatively small influence on the elastic stiffness, the Stone-Wales (Figure 5) transformation plays a key-role in the nanotube plastic deformation under tension. This transformation corresponds to a reversible diatomic interchange where the resulting structure is built upon two pentagons and two heptagons in pairs.

In the MWCNTs (Russian doll model), each individual concentric tube can have different chirality. This primary symmetric classification of CNTs is very important because variations in the nanotube morphology can lead to changes in the properties of the nanotube. For example, the structure of a CNT determines its electronic behaviour. Indeed, the electronic properties of a nanotube follow a general rule: if  $(n-m)$  is a multiple of 3, then the tube exhibits a metallic behaviour, otherwise it is an electrical semiconductor [18]. Investigations of the influence of chirality on the mechanical properties of CNTs have also been reported. So, armchair nanotubes present a metallic behaviour while zig-zag and chiral nanotubes can be either metallic or semiconducting [19]. Although the chirality has a relatively small influence on the elastic stiffness, the Stone-Wales (Figure 5) transformation plays a key-role in the nanotube plastic deformation under tension. This transformation corresponds to a reversible diatomic interchange where the resulting structure is built upon two pentagons and two heptagons in pairs.

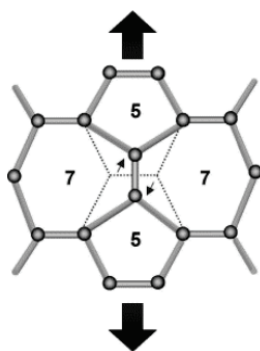


**Figure 5.** The Stone-Wales transformation occurring in an armchair nanotube under axial tension [10].

The Stone-Wales transformation introduces a new defect in the nanotube structure, the heptagon. Heptagons allow for concave areas within the nanotube. Thus, the heptagonal defects in nanotubes can result in many possible equilibrium shapes. Indeed, most nanotubes are not straight cylinders with hemispherical caps.

## 2.3 Nitrogen containing CNT

The first studies analyzing the doping effects on CNTs appeared in 1993 [20], not much later than Iijima's reports on transmission electron microscopy observations were first published [7]. This is just one of the many examples that inspired the investigation of CNT doping.

The insertion of N into a CNT lattice changes the overall structure of the CNT and thus affects both the physical and chemical properties of the nanotubes. Particularly incorporation of nitrogen in CNT received much attention due to enhanced conductivity as compared to their undoped counterparts. Several reports in literature suggest NCNT to be suitable as field emission devices due to the presence of donor states just above the Fermi level [21, 22]. Also, a few reports deal with the catalytic potential of NCNT mainly describing indirect use of NCNT to enhance catalytic performance.

The atomic dimensions of carbon, nitrogen and oxygen as well as the bond length in aromatic structures do not differ very much which makes the latter two elements very suitable for incorporation into the graphene layers of CNT. However, the C-N bond is shorter as compared to the C-C and C-O bond lengths. Incorporation of nitrogen into the CNT may therefore distort a perfectly ordered graphitic matrix. It was shown that low concentrations of nitrogen, i.e.,  $N/C < 0.17$ , can be incorporated in the graphene layer without changing the

graphitic properties and tube morphology too much (Figure 6a) [23]. However, above this level nitrogen is incorporated in pentagons which cause the curving of basal planes as is illustrated in Figure 6b.

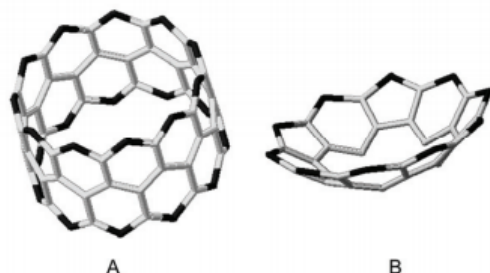


**Figure 6.** Curvature of graphene layer (gray lines C, black lines N) as consequence of N/C ratio; N/C = 0.17 (a) and N/C = 0.40 (b) [23].

Thus nitrogen is able to release strain in the structure of the NCNT, this might be the reason why nitrogen is found around defects [24] and why their concentration in the inner layers was found to be higher than in the outer layers [25]. The position of heteroatoms in the CNTs network must not exclusively be substitutional to affect the properties of the structures. In fact, the properties of nanoscopic objects depend crucially on the position of each atom [26, 27, 28]. Bearing in mind that N contains one additional electron as compared to C, novel electronic properties can be expected if N atoms directly substitute C atoms in the graphitic lattice and one could anticipate that they would generate an n-type material [29]. However, a direct substitution of the C atoms is not the only possibility to incorporate N in the nanotube assembly. Due to its size, N can also generate a defect in the tube structure keeping the heteroatoms on the walls, requiring a rearrangement of the neighboring C atoms. In this case the n-type behavior is not immediately inferred. The electronic behavior depends on the new geometry which involves a different wall structure, and one cannot discard that this new arrangement makes a p-type doping also feasible. Defects, direct substitution of heteroatoms and atom rearrangements are the so-called on-wall dopants.

At least three types of nitrogen are found in NCNT. These are pyridinic nitrogen, pyrrolic nitrogen and quaternary nitrogen [30, 31]. The pyridinic N type is an  $sp^2$  hybridized nitrogen atom located at the edges or at defects of the graphene sheets (Figure 7a) [22]. These pyridinic nitrogen atoms have a localized electron lone pair which are active in base catalyzed reactions [32]. Therefore the optimization of the amount of pyridinic nitrogen is important for catalysis. The pyrrolic N type is  $sp^3$  hybridized and part of a five membered ring structure (Figure 7b). The quaternary N is a carbon substituted nitrogen atom located in the graphene sheet (Figure 7c). A fourth type has been reported and labeled as N–X species (Figure 7d), believed to be an oxidized type of pyridinic N.



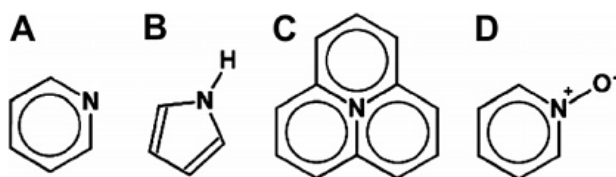


**Figure 7.** Types of nitrogen species found in NCNT: (a) pyridinic, (b) pyrrolic, (c) quaternary and (d) oxidized pyridinic [33].

Nitrogen atoms incorporated in the CNT structure represent for several reasons a practical and illustrative case. If a SWCNT is doped with a foreign N atom, its outstanding electronic properties differ drastically from an undoped SWCNT. Even the cases of multiwalled and C-SWNTs doped with N are radically different. As compared to bulk doped carbons and also against other doped carbon layered structures, (i.e. bulk doped graphite), the electronic properties of CNTs differ due to quantum confinement effects and the curvature of the cylinders.

### **3. CARBON NANOTUBES: METHODS OF PRODUCTION**

The morphology and properties of CNTs are closely related to their method of production. The first developed production methods were the arc discharge and laser vaporization processes. However, majority of works has been devoted to CVD techniques since they can be readily scaled up for industrial production.

#### **3.1. Arc discharge**

The arc discharge method utilizes an electric arc discharge between two graphite electrodes in an inert gas atmosphere (e.g. argon or helium) [34]. This method requires very high temperatures ( $>5000^{\circ}\text{C}$ ) and produces a mixture of different carbon structures, including fullerenes, onion-like carbon particles and some graphite sheets. It is necessary to separate CNTs from the soot and catalytic metals present in the crude product. Although it is possible to selectively grow SWNTs or MWNTs, CNTs produced by this method are normally entangled with poor control over the length and diameter [35].

#### **3.2. Laser Ablation Technique**

The first fullerenes were synthesized with the laser ablation technique developed by Kroto and Smalley [6]. The same approach can be used to produce CNT's within an inert atmosphere (helium or argon). In this method carbon from a solid disk of graphite is vaporized by laser irradiation. The graphite target is placed in the middle of an evacuated long quartz tube and first heated to  $1200^{\circ}\text{C}$ . The tube is then filled with a flowing inert gas and a laser beam, focused on the graphite target, is scanned across the surface to maintain an uniform vaporization rate. The ejected carbon fragments are swept by the flowing gas from the high-temperature zone downstream and deposited on a water-cooled copper collector at the end of the apparatus and at the walls of the quartz tube (Figure 8) The deposited material consist of MWNTs (4–24 graphitic layers, and length of 300 nm) when using pure graphite, and perfectly closed SWNT's arranged in ropes (5–20 nm in diameter and several hundreds of  $\mu\text{m}$  in length) when small amount of transition metal has been added to the carbon target. To improve the method a second laser pulse is used to provide more uniform vaporization and to minimize the amount of carbon deposited as soot.

However, as for the arc discharge technique, the quantities of the produced sample are limited by the size of the used carbon source. In addition, subsequent purification steps are necessary to separate the nanotubes from undesirable by-products. These limitations have motivated the development of gas-phase techniques, such as CVD.

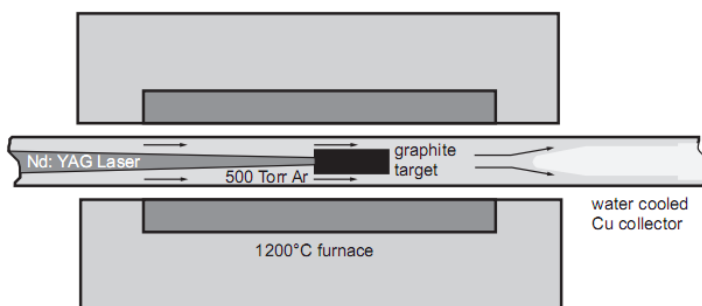


**Figure 8.** Schematic illustration of a laser ablation apparatus [36].

### 3.3. Chemical Vapor Deposition

The formation of carbon filaments from the catalytic decomposition of carbon-containing gas over metal surfaces has been known for a long time [2, 5, 37]. However today, the catalytic CVD method is considered as the only economically viable process for large-scale CNT production and the integration of CNTs into various devices [38] as it is shown by the large-scale production of quite pure CNTs by some companies [39].

When carbon-containing gases such as acetylene ( $C_2H_2$ ), methane ( $CH_4$ ), benzene ( $C_6H_6$ ) or carbon monoxide are decomposed over metal surfaces (Fe, Ni, Co, ...) at temperatures between 500°C and 1100°C the liberated carbon atoms may form CNTs. The CVD process has several advantages over other synthesis methods. CNT's can grow at a relatively low temperature and their size, growth rate, diameter, length and crystallinity can be manipulated by changing the type and morphology of the catalysts. The CVD method allows also the growth of well aligned nanotubes [40], the fabrication of high quality SWCNTs [41] and MWCNTs with specific properties [42]. CVD synthesis may result in individual well dispersed nanotubes grown directly onto substrates or in bulk masses. A major advantage of CVD is that the nanotubes can be used directly without further purification unless removal of the catalyst particle is necessary. Several modifications of the CVD method exist and are thermal hot-wall CVD, cold-wall CVD, Plasma Enhanced Chemical Vapour Deposition (PECVD) etc.

### 3.4. Hot wall CVD reactor

A simple reactor consists from quartz tube inserted into tubular electric furnace (Figure 9). The furnace is typically heated to 600–1100°C depending from the used method. The main characteristic feature of this method is that the gas mixture is heated before reaching the catalyst. The result of the heating can be

partial decomposition of the gas that leads to appearance of new compounds that sometimes cause several unwanted effects. Cold-wall reactors were introduced to avoid this unwanted prior heating of the gas or at least gaining more control over the process.

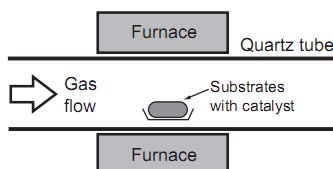


**Figure 9.** Horizontal hot-wall CVD furnace used to grow CNTs [37].

### 3.5. Cold-wall CVD reactor

Typical cold-wall CVD reactor consists of main chamber where a substrate heater is situated. The reactor can be either vertical or horizontal configuration. Sometimes it can be equipped with preheater for gas activation (Figure 10).

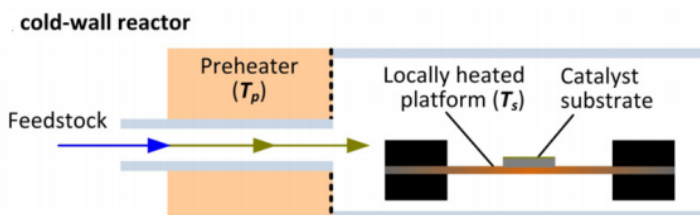


**Figure 10.** Horizontal cold-wall CVD reactor [43].

In PECVD the same construction principles are used but for gas activation DC- (direct current), RF- (radio frequency) or MW-plasma (micro wave) excitations are used. Also in PECVD lower gas pressures are frequently used.

## 4. CARBON NANOTUBE GROWTH MECHANISM DURING CVD

CNT growth mechanism has been debatable right from its discovery. Based on the reaction conditions and post-deposition product analyses, several groups have proposed different possibilities, which are often contradicting. Therefore, no single CNT growth mechanism is well established till date [44]. Nevertheless, widely-accepted most general mechanism can be outlined as follows. Hydrocarbon vapor when comes in contact with the “hot” metal nanoparticles, first decomposes into carbon and hydrogen species; hydrogen flies away and carbon gets dissolved into the metal. After reaching the carbon-solubility limit in the metal at that temperature, as-dissolved carbon precipitates out and crystallizes in the form of a cylindrical network having no dangling bonds and hence energetically stable. Hydrocarbon decomposition (being an exothermic process) releases some heat to the metal’s exposed zone, while carbon crystallization (being an endothermic process) absorbs some heat from the metal’s precipitation zone. This precise thermal gradient inside the metal particle keeps the process on. Now there are two general cases. When the catalyst–substrate interaction is weak (metal has an acute contact angle with the substrate), hydrocarbon decomposes on the top surface of the metal, carbon diffuses down through the metal, and CNT precipitates out across the metal bottom (Figure 11), pushing the whole metal particle off the substrate (as depicted in step (i)).

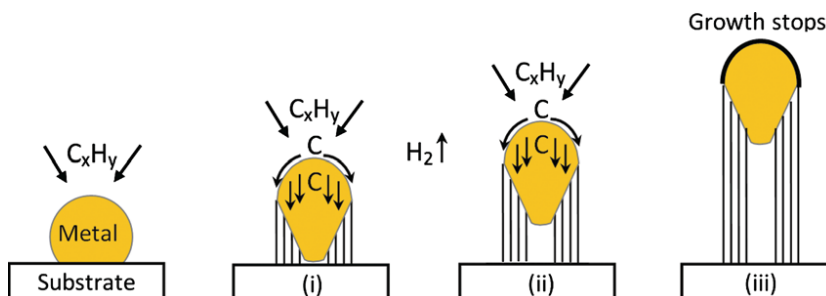


**Figure 11.** Widely-accepted growth mechanisms for CNTs tip-growth model [44].

As long as the metal’s top is open for fresh hydrocarbon decomposition (concentration gradient exists in the metal allowing carbon diffusion), CNT continues to grow longer and longer (ii). Once the metal is fully covered with excess carbon, its catalytic activity ceases and the CNT growth is stopped (iii). This is known as “tip-growth model.” [45] In the other case, (Figure 12) when the catalyst – substrate interaction is strong (metal has an obtuse contact angle with the substrate), initial hydrocarbon decomposition and carbon diffusion take place similar to that in the tip-growth case, but the CNT precipitation fails to

push the metal particle up; so the precipitation is compelled to emerge out from the metal's apex (farthest from the substrate, having minimum interaction with the substrate).

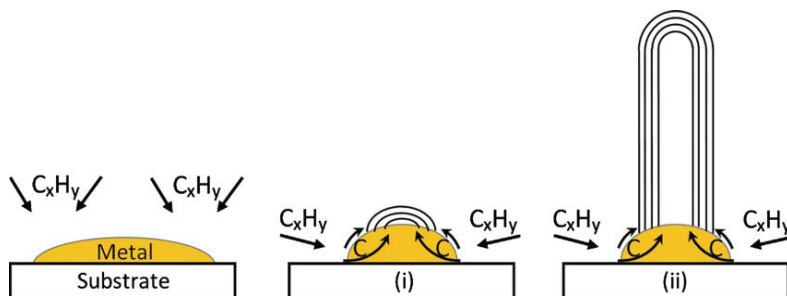


**Figure 12.** Widely-accepted growth mechanisms for CNTs base-growth model [44].

First, carbon crystallizes out as a hemispherical dome (the most favourable closed-carbon network on a spherical nanoparticle) which then extends up in the form of seamless graphitic cylinder. Subsequent hydrocarbon deposition takes place on the lower peripheral surface of the metal, and as dissolved carbon diffuses upward. Thus CNT grows up with the catalyst particle rooted on its base; hence, this is known as “base-growth model” [46]. Formation of single- or multi-wall CNT is governed by the size of the catalyst particle [47]. Broadly speaking, when the particle size is a few nm, SWCNT forms; whereas particles – a few tens nm wide – favour MWCNT formation. CNT synthesis involves many parameters such as hydrocarbon, catalyst, temperature, pressure, gas-flow rate, deposition time, reactor geometry. Despite tremendous progress in yields, lowering of the synthesis costs and the improved purity of the products obtained by CVD, there is still much debate about what really controls the growth of CNT's.

## 4.1. Synthesis of nitrogen-containing nanotubes

NCNT can be obtained by post synthesis modification of CNT with nitrogen containing organic molecules [48, 49, 50], incorporation of nitrogen during synthesis of the CNT for example by pyrolysis of N-containing organo-metallic compounds sometimes in the presence of an additional C/N source [51, 52] or chemical vapour deposition of N-containing organic compounds over a supported transition metal based catalyst [53, 25, 54]. With high temperature techniques, such as laser ablation, arc discharge and magnetron sputtering, a large percentage of N incorporation, up to 33%, has been achieved, whereas with low temperature techniques, viz. CVD and pyrolysis, up to 20% has been realized. However not always the main goal is to incorporate as much nitrogen

as possible. In some application the structure of incorporated nitrogen is very important, for example in electrochemical oxygen reduction within fuel cell, where pyridinic form of incorporated nitrogen is the main factor responsible for enhanced electrochemical activity [55]. Pyridinic nitrogen concentration is greater in nanotubes produced at lower temperatures [56].

## **5. FUNCTIONALIZATION OF CARBON NANOTUBES**

### **5.1. Interests and types of functionalization**

Pristine CNTs are insoluble in many liquids such as water, polymer resins, and most solvents. CNTs are both highly polarizable and smooth-sided compounds. Individual tubes attract each other with an attractive force of 0.5 eV/nm. Due to high cohesive interactions, CNTs having large molecular weights appear as bundled structures or ropes [57]. This characteristic of CNTs gives rise to low solubility and poor dispersion in common organic solvents, aqueous solutions and polymeric matrices. Another factor affecting dispersion quality is the lack of interfacial interactions between a nanotube and the solvent. This means they are difficult to evenly disperse in a liquid matrix such as epoxies and other polymers, complicating efforts to utilize CNTs outstanding physical properties in nanocomposite materials, as well as in other practical nanotechnology applications which require preparation of uniform mixtures of CNTs with many different organic, inorganic, and polymeric materials. To make nanotubes more easily dispersible in liquids, it is necessary to physically or chemically attach certain molecules, or functional groups, to their sidewalls without significantly changing the nanotubes desirable properties.

Introduction of surface groups has the obvious advantage of introducing extra functionality to the CNTs which can be important for sensing, self assembly in electronic devices or even as points of attachment for polymers or biomolecules [58]. Also the surface groups have additional advantage of interrupting the strong Van der Waals forces that cause aggregation or bundling of the CNTs, particularly problematic for SWNTs and thus aid dispersion in both aqueous and non-aqueous solvents [59]. Several strategies including covalent and non-covalent techniques have been developed to overcome the solubility problem and to produce reactive side groups which could interact with different systems (Figure 13). Methods for noncovalent [60], [61], [62] and covalent [60], [62], [63], [64] functionalization of SWNTs have recently been reviewed.



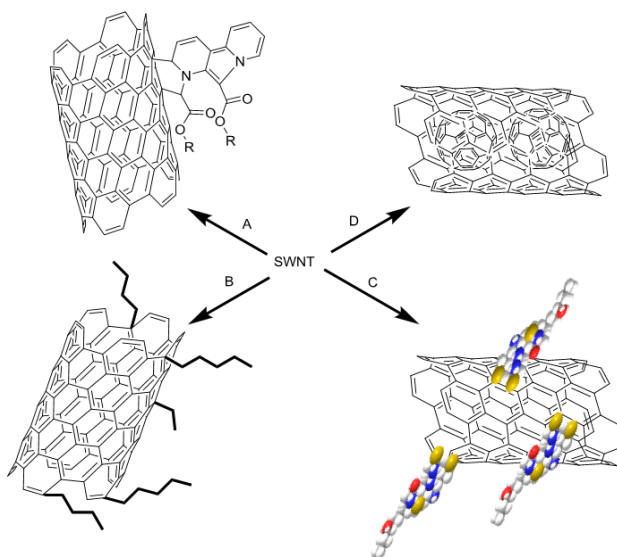


**Figure 13.** Functionalization possibilities for SWNTs: a) covalent sidewall functionalization, b) defect-group functionalization, c) non-covalent hexahedral functionalization with surfactants or polymers, d) endohedral functionalization with, for example,  $C_{60}$ . For methods b-c, the groups attached to nanotube surface are representative [58].

## 5.2. Non-covalent functionalization with surfactants or polymers

In comparison to a covalent bond, the energy released in the formation of a non-covalent bond is lower. However, in supramolecular systems like CNTs, the number of these bonds can be high and become dominant. The noncovalent interaction is based on Van der Waals forces or  $\pi$ - $\pi$  stacking and it is controlled by thermodynamics. The great advantage of this type of functionalization relies upon the possibility of attaching various groups without disturbing the  $\pi$  electronic system of the rolled graphene sheets of CNTs [65].

The major disadvantage of non-covalent routes for the modification of CNTs is that they can make large portions of the CNT surface inaccessible, which could be a disadvantage for applications such as electronics. Non-covalent functionalization of CNTs using surfactants such as sodium dodecyl sulphate, [66], [67] sodium dodecylbenzene sulphonate [68], cationic surfactants such as benzalkonium chloride [69], and non-ionic surfactants such as Triton-X [69] has widely been used to prepare stable dispersions of de-bundled CNTs. Treatment of CNTs with polymer matrixes including polystyrene sulphonate and polyvinyl pyrrolidone resulted in highly soluble CNTs [57]. Solubility of CNTs has also been enhanced using different polymers such as poly(acrylic acid),

polyethylene, poly(dimethylsiloxane), and natural polymers, such as Gum Arabic 88 and starch. It has been reported that CNTs could be non-covalently modified to increase solubility and processability in water using proteins and DNA [70]. It has also been shown that biomolecules for biosensor development and large aromatic compounds such as pyrene could be used for the non-covalent functionalization of CNTs.

### 5.3. Covalent Functionalization of Carbon Nanotubes

Two major groups of chemical functionalization of CNTs via covalent attachment can be distinguished, the end and “defect-group” chemistry, and the sidewall functionalization.

#### End and defect-side chemistry

The functionalization via “end and defect-side” chemistry grafts a functional group directly on the already existing defects in the structure of CNTs. Indeed, CNTs are generally described as perfect graphite sheets rolled into nanocylinders. In reality, all CNTs present defects and can be curved. Typically, around 1–3% of carbon atoms of a nanotube are located at a defect site [71].

The end caps of nanotubes can be composed of highly curved fullerene-like hemispheres, which are highly reactive as compared to the sidewalls [72]. The sidewalls themselves contain defect sites such as pentagon-heptagon pairs called Stone-Wales defects,  $sp^3$ -hybridized defects and vacancies in the nanotube lattice [73]. The most frequently encountered type of defect is Stone-Wales defect which leads to a local deformation of the nanotube curvature. Addition reactions are most favored at the carbon-carbon double bonds in these positions. The different typical defects are showed in the (Figure 14) [60].

Five- or seven- membered rings in the carbon framework, instead of the normal six-membered rings, lead to a bend in the tube (Figure 14, arrow “A”). The  $sp^3$ -hybridized defects are indicated with the letter B (R=H and OH). Carbon framework can be damaged by oxidative conditions, which leaves e.g. –COOH groups on the edge of a hole (Figure 14, “C”). Figure 14 “D” shows open end of the SWNT terminated with e.g. –COOH groups. Other terminal groups, such as –OH, -H and =O, are also possible.

Frequently, these intrinsic defects are supplemented by oxidative damages to the nanotube framework by strong acids during the purification step. These acids leave vacancies functionalized with oxygenated functional groups such as carboxylic acid, ketone, alcohol and ester groups [74]. The oxidative introduced carboxyl groups represent useful sites for further modifications in organic solvents such as the coupling of molecules through the creation of amide and ester bonds. One advantage of the defect-side chemistry is that functionalized CNT retain their pristine electronic and mechanical properties [75]. However, the repartition of grafted functions is not homogenous along CNTs. Indeed, the

carboxylic groups, used as anchoring sites, are placed in majority at the extremities of CNT.

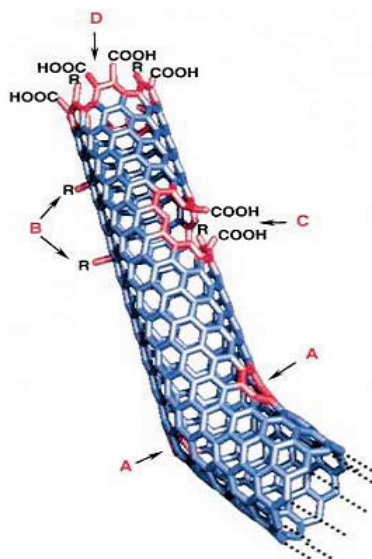


**Figure 14.** Typical defects in a SWNT [60]. (marks A-D are explained in the text)

### Sidewall functionalization

Covalent functionalization of SWNTs produces  $sp^3$  hybridized carbon atoms on the side wall. The common aspect of each functionalization method is the use of highly reactive species to attack nanotube sidewalls. Functionalization occurs at defect sites along the sidewalls and tube ends, which are also easily oxidized to form open tubes. Hence, covalent functionalization increases the solubility and processability of CNT. However, it may distort or destroy the unique properties of the nanotube network.

The first covalent sidewall functionalization was carried out on the basis of well-developed addition chemistry on fullerenes. However, it is predicted that the sidewall addition chemistry of CNTs differs from that of fullerenes, even though both are curved, conjugated carbon systems [76]. Indeed, the chemical reactivity in strained carbon systems arises from two factors, the pyramidalization at the carbon atoms and the  $\pi$ -orbital misalignment between adjacent carbon atoms [77]. In fullerenes, the former is the most influent factor due to their pronounced curvature. The relief of pyramidalization strain energy results in energetically favourable addition reactions onto fullerene structures. In CNT, the pyramidalization strain is not as acute and  $\pi$ -orbital misalignment is expected to have a greater influence [78]. This misalignment, associated with bonds at an angle to the tube circumference (bonds that are not perpendicular or parallel to the tube axis), is the origin of torsional strain in CNTs. The relief of

this strain controls the extent of reactivity of CNT. These two factors influencing the reactivity of CNTs are represented in Figure 15. It can be observed that the C-C bond in CNTs structure will be more or less reactive as function of its angle in to the tube circumference. The strain in CNTs arises thus from these factors which scale inversely with tube diameter [60], thinner CNTs are more reactive than larger tubes. However, the reactivity of CNT sidewalls remains low and sidewall-functionalization is only successful if a highly reactive reagent is used, whereas the nanotube caps are quite reactive due to their fullerene-like structure. Another constraint for sidewall functionalization is the tendency of CNTs to form bundles and to limit the available nanotube surface for the grafting of chemical reagents.

A large majority of covalent sidewall functionalization is carried out in organic solvents, which allows the utilization of sonication process to improve the dispersion of CNTs and, thus, the available surface of carbon nanotubes. However, precipitation immediately occurs when this process is interrupted [62]. The required reactive species such as carbenes, nitrenes or radicals, are in general made available through thermally activated reactions [79]. However, the addition mechanisms are not understood completely yet. Normally, the addition reaction could be initiated exclusively on the intact sidewall or in parallel at defect sites. Several covalent functionalization methods are available such as defect site production using acids [66], [80] and functionalization from the defects, producing carboxylic acid groups on the end caps and subsequent reactions from the acids [81], [82] and direct covalent sidewall functionalization [64].

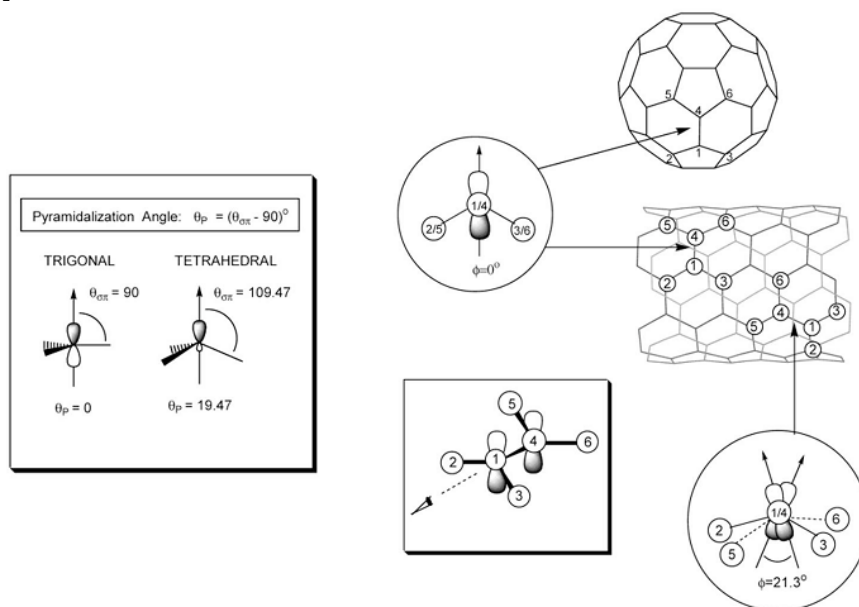


**Figure 15.** Pyramidalization angles ( $\theta_p$ ) and the  $\pi$ -orbital misalignment angles ( $\phi$ ) along C1-C4 in the (5,5) SWNT and its capping fullerene C<sub>60</sub> [63].

However, CNT functionalization carried out in organic solvent present some inconvenients. The first one is the necessity to agitate CNT by sonication process to get a good dispersion of them in organic solvent. Indeed, intensive or too long sonication causes severe damages to the tube walls and the average length of CNTs can be reduced [83]. Secondly, this functionalization inorganic solvent requires generally multistep time-consuming reactions. Finally, the use of organic solvent is polluting and difficult to upgrade for industrial processes.

To overcome the drawbacks of the wet chemistry functionalization, “dry” processes are being developed. The ball-milling of MWNTs in reactive atmospheres was shown to functionalize nanotubes with different chemical groups, such as amides, carbonyls, thiols and mercaptans for instance, depending on the used atmosphere [84]. Using this method, CNTs are broken and radicals formed on their newly created extremities can then react with the introduced gas. A relatively long time (min. 24h) is necessary to get an enough quantity of functions onto CNTs. However, the average length of CNTs decreases for increasing treatment and amorphous carbon is observed after the breaking process [85]. Another drawback is the presence of functional groups exclusively on the ends of cup-stacked CNTs.

To avoid above-mentioned problems several methods utilizing gas-phase treatments are proposed. Conventional gas-phase treatment methods employ exposure of CNTs to air, ozone, 86 or oxygen plasma 87 and are typically less effective than wet acid-treatments 88. Moreover, in the case of using plasma or ozone, complicated devices are needed. Xia *et al* 89 showed that application of acid vapors could be a promising gas phase route for CNTs functionalization. They applied the method for successful functionalization of a powder of CNTs with diameters in the range of 50–200 nm. However, until now no data was available about applicability of this treatment on smaller diameters nanotubes and evidence of functionalization of aligned arrays of CNTs (s.c. “supergrowth” CNTs).

## 6. CHARACTERIZATION METHODS

### 6.1. Scanning Electron Microscopy

The (SEM) is one of the most versatile instruments widely applied to surface microstructure imaging. SEM is a type of electron microscopy that images the sample surface of a solid specimen by using a focused beam of high-energy electrons. The signal contains information about surface topography, external morphology, chemical composition, crystallographic information, and electrical conductivity.

The combination of high magnification, large depth of focus, excellent resolution, and ease of sample observation makes the SEM one of the most heavily used instruments in research areas of nanoscience and –technology [90].

### 6.2. Fundamental principles

Electron microscopes operate exactly as optical microscopes do with the exception being that they focus a beam of electrons instead of a beam of light to image the specimen and gain information about its structure and composition. The electron microscope takes advantage of the wave nature of rapidly moving electrons. Visible light has wavelengths from 400 to 700 nm, where as electrons accelerated to 10 keV have the wavelength of 0.12 Å.

The scanning process and image formation in SEM depends on signals produced from elastic and inelastic interactions between the high energy electron beam and the specimen surface (Figure 16). When the primary electron beam bombards the sample surface, energetic electrons penetrate into the sample surface forming an excitation zone, known as the interaction volume

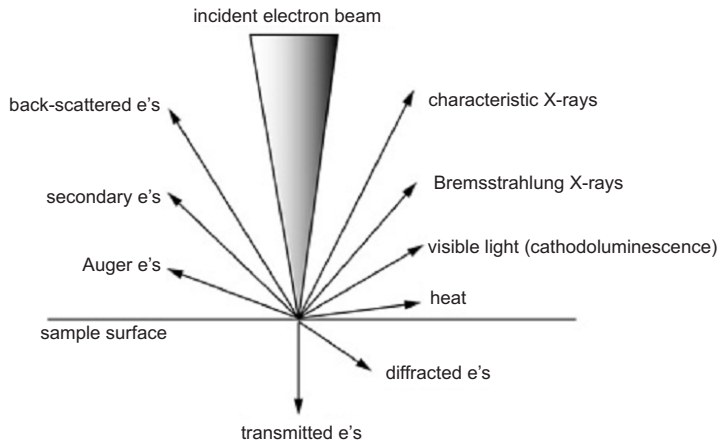


**Figure 16.** Schematic of signals generated by the electron beam–specimen interaction in the SEM [91].

before they collide with the specimen atom (Figure 17). The shape and size of the interaction volume depends on the accelerating voltage and atomic number. In the process, the electrons also lose energy by repeated, random scattering. Elastic scattering occurs from the deflection of incident electrons by the atomic nucleus or outer shell electrons [92]. This accounts for the negligible energy loss and produces backscattered electrons at an angle of more than  $90^\circ$ .

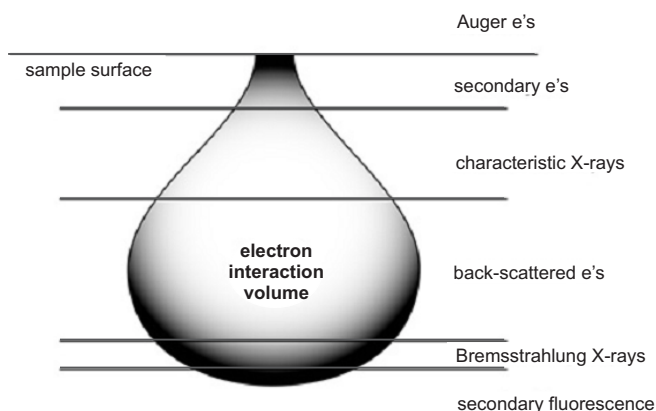
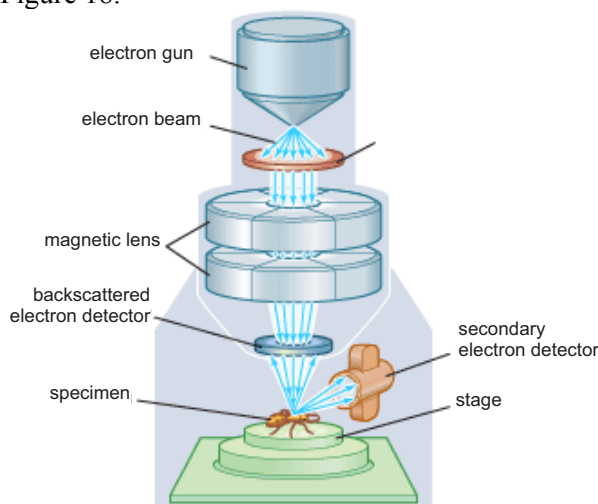


**Figure 17.** Electron interaction volume within a sample [106].

Inelastic scattering transfers substantial amounts of energy to emit secondary electrons. In addition to those signals, a number of other signals such as Auger electrons, characteristic X-rays, cathodoluminescence, transmitted electrons, and specimen currents are emitted (Figure 16). Schematic diagram of a SEM is represented at Figure 18.



© 2008 Encyclopaedia Britannica, inc.

**Figure 18.** Schematic diagram of a scanning electron microscope [93].

### 6.3. Energy Dispersive Spectroscopy

EDS [94] is a chemical analysis technique that allows a microscopist to determine the concentration of most elemental species in a given sample. The fundamental principle behind this method is the emission and detection of x-rays from a given sampling volume that are characteristic to specific elements. A material can produce x-rays when bombarded with high-energy electrons. Assuming the Bohr model for an atom, the electron beam excites the inner k-shell electrons sufficiently to eject an electron and produce a hole in the k-shell. The atom is then left in an excited, or ionized, state. To compensate, an electron from the outer shells will fill the inner shell hole and it is this transition that will emit an x-ray with energy equal to that between the two electron states, as shown in Figure 19.

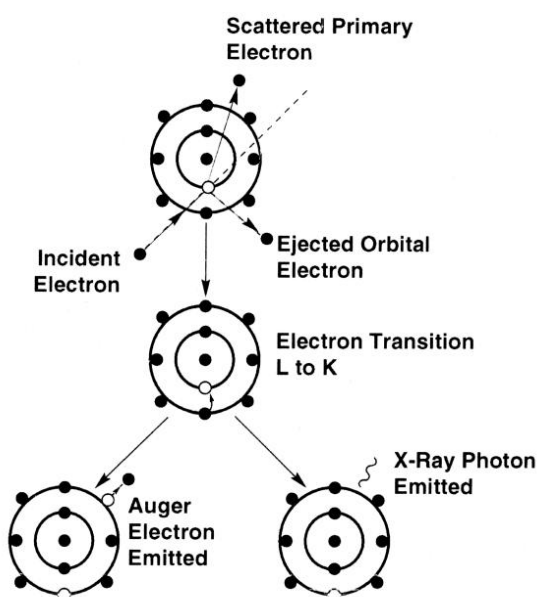


**Figure 19.** X-ray and Auger electron emission through electron transition resulting from ejected k-shell electron [94].

The wavelength of the x-ray emitted is characteristic to that respective element and allows for chemical identification. Since each element has x-rays that have specific energies, the chemical composition can be obtained by integrating the area under the intensity peak. The output for an EDS analysis is a plot of intensity or x-ray counts vs. characteristic energy in electron volts (eV).



## 6.4. X-Ray Photoelectron Spectroscopy (XPS)

XPS is a very informative surface chemical analysis technique that can be used to analyze the surface chemistry of the material [95]. It provides a wealth of information related to elemental composition, chemical state and electronic state of the elements present in a sample. It utilizes x-rays with low energy (typically 1–2 keV) to knock off photoelectrons from atoms of the sample through the photoelectric effect. The energy content of these ejected electrons is then analyzed by a spectrometer to identify the elements where they came from [96]. The binding energies of core electrons are highly characteristic of the element present in sample. Small “chemical shifts” in binding energies give information about the surrounding chemical environment of an atom, allowing deductions to be made about the chemical structure of the sample [97]. A schematics of a XPS setup is shown in Figure 20.

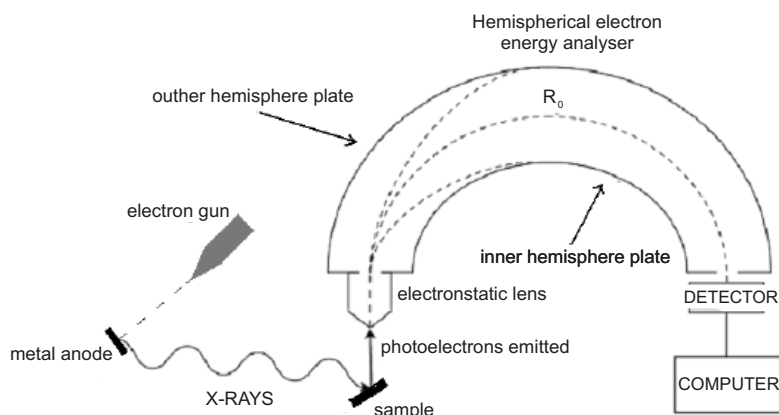


**Figure 20.** Schematic diagram illustrating the basic design of an x-ray photoelectron spectrometer [95].

## **7. SYNTHESIS OF MILLIMETER SCALE ALIGNED CARBON NANOTUBES: EXPERIMENTAL RESULTS (Paper – V)**

The aim of this chapter is to provide an overview of the main results of development of methods to grow millimeter scale ACNTs. The experimental methods and set-ups, and the main process steps used to synthesize CNTs samples will be described. ACNTs are synthesized by using a catalytic CVD. In particular, the focus has been addressed to the implementation of a deposition process that can produce well oriented, long and thin CNTs. All the synthesis processes have been achieved at the Institute of Physics University of Tartu.

### **7.1. Preparation of Catalyst Layers**

Polished silicon wafers were chosen as substrate for synthesis of ACNT, due to thermal stability, ability to form silicon oxide and flat surface, which is very important for suitable distribution of catalytic particles and CNT alignment. Silicon substrate was coated with about 120 nm of thermally grown oxide layer. Additionally a few nm of aluminium oxide barrier layer was deposited with magnetron plasma sputtering from aluminium electrode (SC7640 Sputter Coater, Quorum Technologies). XPS and EDS measurements confirmed absence of aluminium in metal state. Aluminium oxide is widely used barrier layer for growing of ACNTs, because of its good adhesion with iron nanoparticles what minimize nanoparticles coarsening and provide “base growth” of CNTs. Also, chemical inertness of aluminium oxide prevents deactivation of iron by reaction with silicon that helps to extend CNTs growth time. Top layer of iron thin film was magnetron sputtered onto aluminium oxide layer. Different combinations of aluminium oxide and iron film thickness were tried, and the combination of 3 nm of  $\text{Al}_2\text{O}_3$  and 1 nm of iron was found the best for our configuration for synthesis of a few millimeter high vertically aligned MWCNTs.

If iron film is exposed to air it oxidizes and for formation of catalytic nanoparticles it needs to be reduced back to metal state. For the reduction usually heating in inert atmosphere with presence of hydrogen is applied. Reduced film melts and forms nanoparticles. Nanoparticles adhesion to substrate, temperature, treatment time, and heating rate play crucial roles in nanoparticles formation with small diameters and narrow diameter distribution.

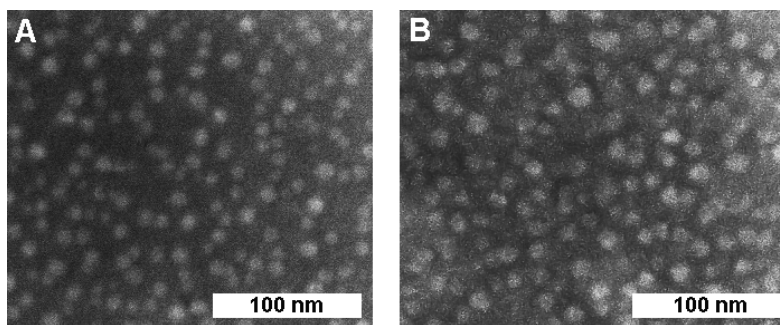


**Figure 21.** Electron microscope images of 1 nm thin film of iron on Si/SiO<sub>2</sub>/Al<sub>2</sub>O<sub>3</sub> layers heated in presence of hydrogen and water for 4 minutes at A) 550°C (particle diameters are about 7–10 nm) and B) 760°C (particle diameters are about 10–13 nm).

For better understanding of the process what leads to iron nanoparticles formation, samples with different iron film thickness was treated in presence of hydrogen at different temperatures (Figure 21) with different treatment times.

Longer times lead to particles coarsening and diameters increasing but insufficient treatment leads to partially reduced particles and decreased catalytical activity. With increasing of iron layer thickness the mean nanoparticle diameter also increase (Figure 22). However, using too thin films may lead to formation of scarce layers of nanoparticles what leads to non-oriented growth of nanotubes.

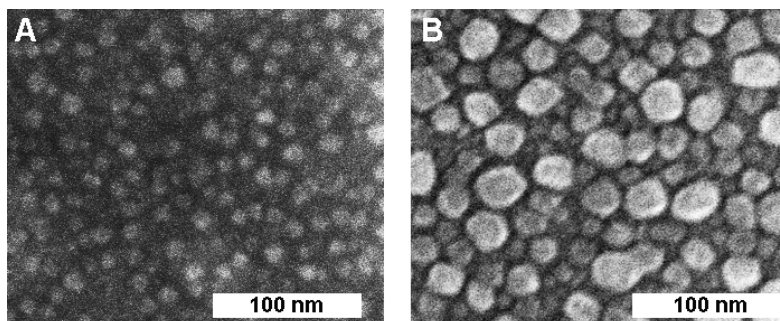


**Figure 22.** Electron microscope images of A) 1 nm (particle diameters are about 10–13 nm) and B) 2 nm (particle diameters are about 13–22 nm) of iron thin film on Si/SiO<sub>2</sub>/Al<sub>2</sub>O<sub>3</sub> layers heated in presence of hydrogen and water for 4 minutes at 760°C.

## 7.2. Experimental setup and synthesis parameters

For synthesis of few millimetre long ACNTs a cold wall CVD reactor was constructed. The cold wall CVD was chosen for fast substrate heating possibilities and for minimizing heating of process gases what simplified the results interpretation and minimize the contamination of the system. Schematically it is drawn in Figure 23. It consists of a high temperature ceramic heater situated inside of a quartz tube. The heater temperature is observed by K-type thermocouple and controlled by a power source. The reaction gases were introduced through the flow meters, which maintain control of the flow speed. Helium was chosen as a carrier gas because of its good diffusion. Hydrogen was used as a reducing agent and at the same time it helps minimize amorphous soot formation on the catalyst particles extending thus the reaction times. Water was used as a weak oxidizer for catalyst life extension as it removes amorphous carbon from the surface of the catalyst particles. Acetylene was used as carbon feedstock. Concentrations and flow speeds of gases were optimized for used catalyst layers. Total flow was typically 200 ml/min.

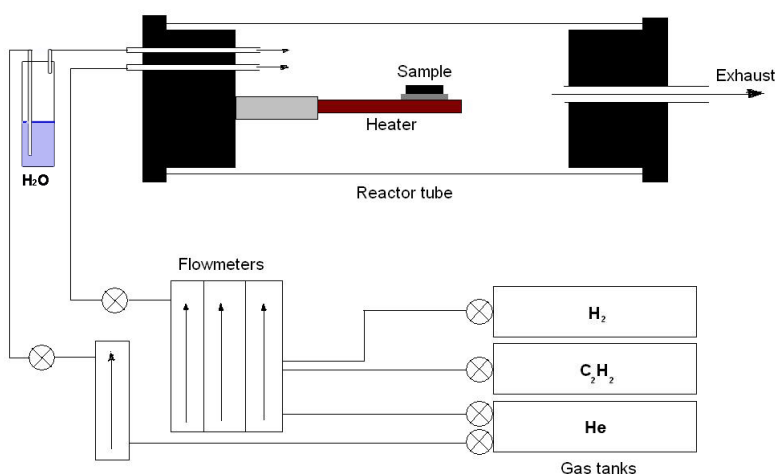


**Figure 23.** Schematically represented cold wall CVD system for ACNTs synthesis.

We tried different proportion of gases (He, H<sub>2</sub> and C<sub>2</sub>H<sub>2</sub>) typically by fixing flow of two gases and varying the flow of the third, and monitoring the ACNT growth. These parameters that gave nanotubes with desirable properties (length and diameter) were fixed and used for further experiments. For catalyst system of SiO<sub>2</sub>/Al<sub>2</sub>O<sub>3</sub>/Fe – 120/3/1 nm the best results were achieved with 49.5% He, 49.5% H<sub>2</sub>, 0.75% C<sub>2</sub>H<sub>2</sub>. At Figure 24 a typical ACNT growth dynamics and length dependence from water vapor concentration can be seen for a given gas mixture and catalyst layer. The dependence is quite strong and significant as

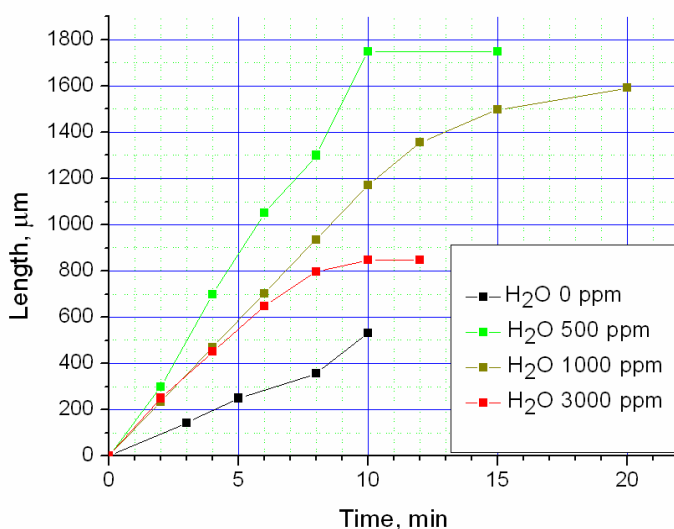


**Figure 24.** Typical ACNT growth dynamics and length dependence (for 49.5% He, 49.5% H<sub>2</sub>, 1% C<sub>2</sub>H<sub>2</sub> mixture with given catalyst layer) from water vapor concentration.

addition addition of 500 ppm of water increases the length of ACNTs by almost three times. This follows from etching nature of water cleaning the catalyst particles from covered amorphous carbon. In contrast, too much water disturbs carbon precipitation onto catalyst and suppresses the growth of CNTs. However, addition of water is not sufficient for initiating infinite growth of CNTs, and there still remain unexplained factors that eventually stop the growth. More parameters need to be optimized to further extend nanotubes length. At Figure 25 a photo of typical ACNT grown on silicon substrate is presented.

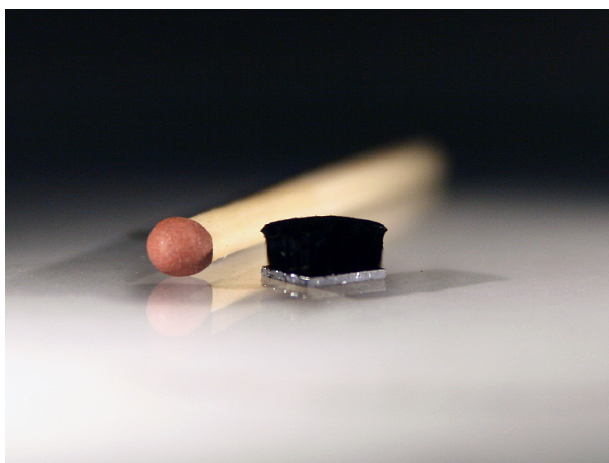


**Figure 25.** Photo of typical ACNT grown on a silicon substrate with catalyst layers.

## 8. SYNTHESIS OF CNT AND NITROGEN DOPED CARBON NANOTUBES ON GLASSY CARBON ELECTRODES: EXPERIMENTAL RESULTS (Paper – I)

### 8.1. Experimental setup

For synthesis of ACNT on GC electrodes a hot wall CVD system was chosen and constructed. The hot wall system helps to maintain uniform sample temperature and helps in acetonitrile decomposition. The system is schematically represented in Figure 26. The hot wall CVD reactor consists of a quartz tube placed inside of a furnace, controlled by temperature controller. With help of a flow meter the gas flow can be controlled. Different methods can be used for mixing necessary gases. We used a simple and effective methods where a carrier gas was let through liquid ethanol or acetonitrile depending on particular application. In some cases mixture of argon and hydrogen were used as carrier gases.

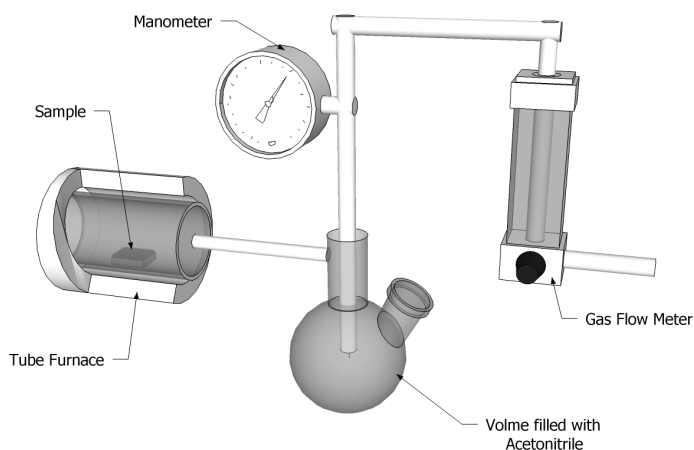


**Figure 26.** Schematics of a CVD system for nitrogen doped CNT synthesis.

During a chemical vapor growth there are a large number of key factors and parameters influencing the nanotubes nucleation and growth and a lot of efforts have been spent to clarify them. In particular the impact of catalyst, substrate, growth temperature, feedstock gas nature, concentration and flow speed parameters were studied for growth process optimization.

## 8.2. Preparation of catalyst materials

There are several methods for catalyst layer preparation for synthesis of vertically aligned CNT. That includes evaporation of thin metal layers, coating with metal salts or direct transfer of metal nanoparticles. Although thin films of metal can give best results in achieving well-dispersed monolayers of nanoparticles it is time consuming, suffers from complexity and difficulties related to uniformity of nanoparticles. Dip or spin coatings of catalyst metal salts are relatively inexpensive and fast methods, however, their drawback is difficulty in producing nanoparticles with desirable diameters. Direct transfer of metal nanoparticles seems very attractive method. Unfortunately, in practice it suffers from complexity of synthesis of nanoparticles with desirable diameters, and even more from difficulties related to subsequent realization of monolayer films of nanoparticles. Keeping in mind potential production technologies the metal salt method was selected for production of catalyst particles. We used a method where in one step solutions of catalyst metal salt and separator salt were spin coated simultaneously onto a substrate. We used cobalt acetate as source of catalyst particles which is one of the most commonly used metal catalysts in CNT synthesis. Aluminium nitrate was used for producing aluminium oxide separator layer below the particles, which is well known substrate for growing of ACNT, due to its chemically inert nature and surface adhesion properties. Although it may seem at the first glance that it seriously limits possible applications of the structures because aluminium oxide is a good electric insulator. However, as seen from our oxygen reduction experiments there are typically enough defects and cracks in the oxide layer covered by conductive material that overall conductivity between CNTs and a substrate is adequate for most applications (Figure 27).

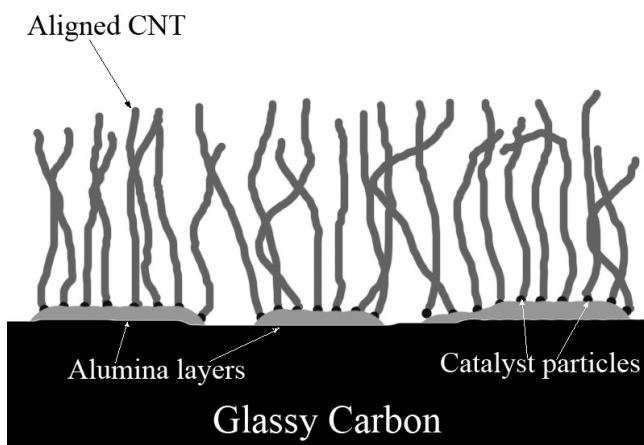


**Figure 27.** Schematically represented catalytic system for growing ACNTs on GC.

At Figure 28 a SEM image of typical cobalt nanoparticles on an aluminium oxide surface is represented.

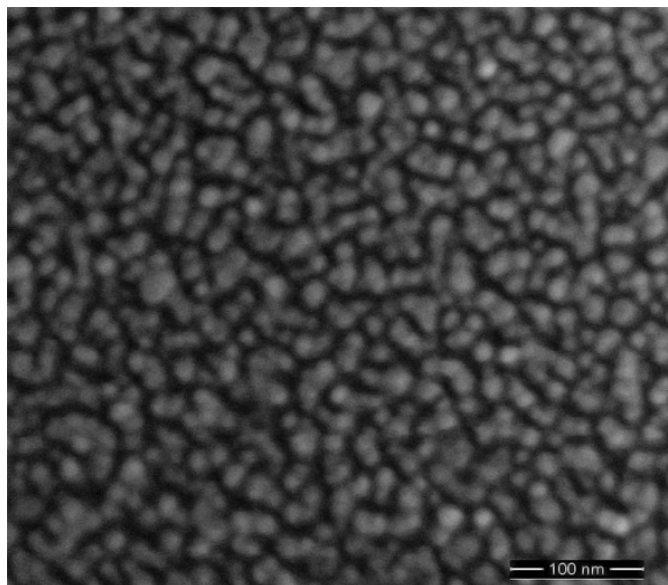


**Figure 28.** SEM image of typical cobalt nanoparticles on aluminium oxide surface.

### **8.3. Synthesis of CNT and nitrogen doped CNT on Glassy Carbon electrodes**

Vertically ACNTs and NCNTs were grown directly on GC electrodes covered with thin film of catalyst using a continuous flow thermal CVD method. Sample was prepared by spin coating of ethanol solution of Co/Al salts directly on the electrode surface.

For the preparation of conventional ACNTs, the electrode was placed on a quartz boat, inside a quartz tube-type electric furnace. The sample was heated up to 800°C in argon at atmospheric pressure. When a set temperature was reached, argon flow of 400 mL/min through bubbler filled with ethanol (99.5%, Aldrich) was supplied. After completion of the reaction, the furnace was turned off and cooled down to room temperature under argon flow. NCNTs were synthesized using the same preparation steps in the same reactor. Acetonitrile (Aldrich) was used both as carbon and nitrogen source. Argon flow rate was the same due to the close values of vapour pressure that ethanol and acetonitrile develop. Reaction temperature of 800°C was chosen (Figure 29) for optimum rate, morphology and impregnation of nitrogen [98], [99]. The temperatures of 700°C (Figure 30) and 750°C did not give enough impregnated nitrogen and tubes prepared at 900°C suffer from morphology problems, larger diameters and



shorter lengths. The GC electrode with layer of aligned NCNTs is shown at Figure 31.

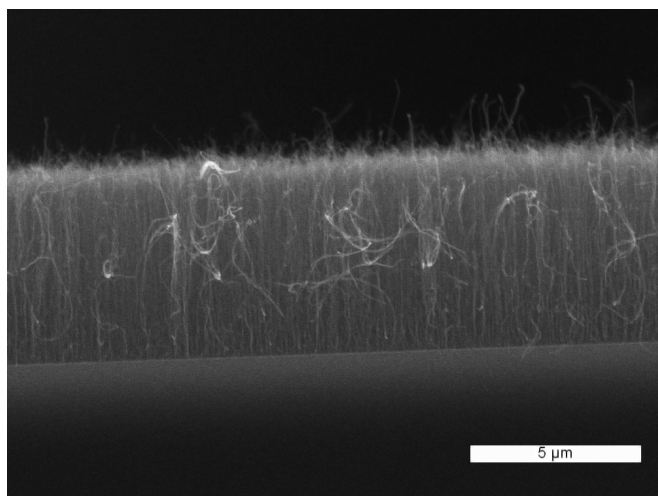


**Figure 29.** Side view of aligned NCNTs synthesized at 800°C.

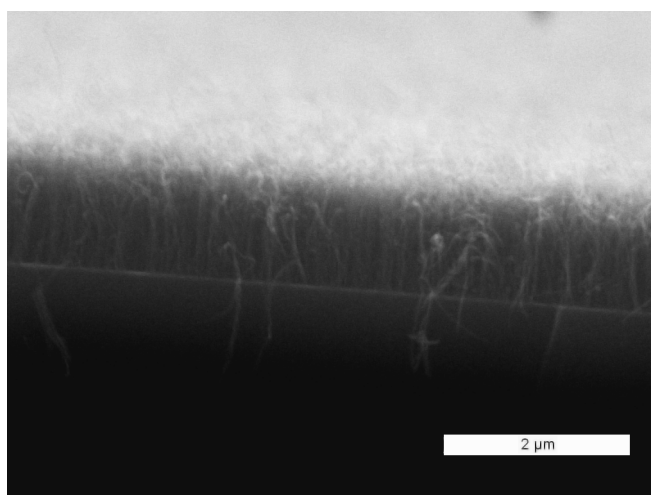


**Figure 30.** Side view of aligned NCNTs synthesized at 700°C.

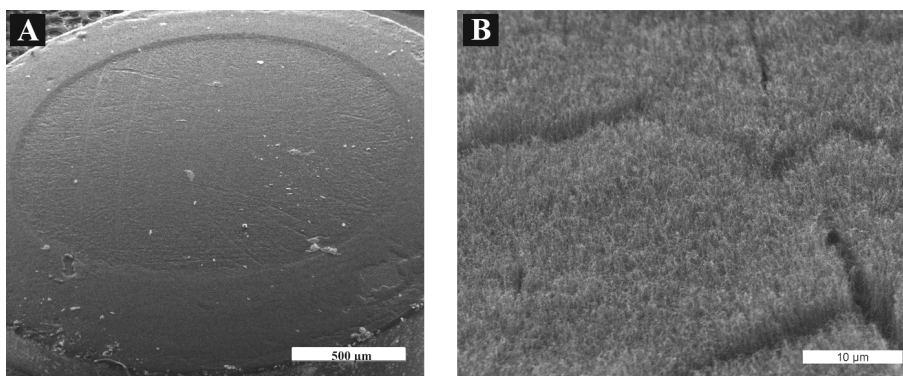


**Figure 31.** The GC electrode with a layer of aligned NCNTs at different magnifications.

## 8.4. Characterisation of NCNT

The XPS measurements were performed to obtain information about the surface composition of NCNTs. For that purpose NCNTs were synthesized on  $12 \times 15 \text{ mm}^2$  and 1 mm thick silicon plates. The XPS experiments were carried out with a SCIENTA SES-100 spectrometer by using an Mg Ka x-ray source. More details could be seen in Paper I.

The C 1s peaks for pure and nitrogen-doped CNTs are presented in Figure 32a. A clear shift of the peaks is observed, demonstrating that some carbon atoms are located in different neighbourhood in case of doped and undoped samples. The N 1s region of XPS spectrum of NCNTs is demonstrated in Figure 32b. It is obvious that the nitrogen signal arises from the NCNT material and not from residual atmospheric nitrogen, since in case of undoped CNTs the N 1s line was not observed. The XPS spectrum of NCNTs in the N 1s region shows at least three different components, which means that nitrogen is linked to several different surroundings (Figure 32b). Two of them are interpreted in the literature as pyridinic-N (398.4 eV) and quaternary-N (400.9 eV) [100]. The origin of the third one at 404.5 eV is not entirely clear. It has been proposed that this peak corresponds to pyridone-N-O (pyridine-N-oxide) [55]. The term “pyridinic” is used to refer N atoms, which contribute to the p-system with one p-electron, whereas quaternary nitrogen corresponds to highly coordinated N atoms substituting inner C atoms on the graphene layers (Figure 7). The nitrogen content (3 at.%) in the surface region of NCNT sample was estimated from XPS experimental data.

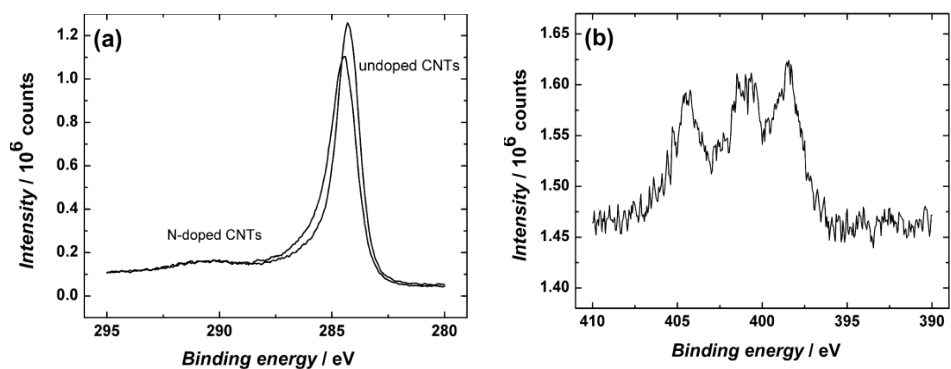


**Figure 32.** High resolution XPS spectra: a) C 1s region for undoped CNTs and NCNTs, b) N 1s region for NCNTs.

## **9. GAS PHASE FUNCTIONALIZATION OF ALIGNED CNT WITH NITRIC ACID VAPOR (Paper – V)**

Despite all advantages of ACNTs their functionalization remains a challenge due to the difficulty of preserving the desirable alignment. Traditional solution-based functionalization protocols involve use of solvents and dispersion of nanotubes, which usually result in the disruption of the aligned structure [101]. The alignment can be preserved using aldehyde plasma vapor deposition [102] and plasma oxidation [103]. However, these processes face problems mentioned before.

In this paper we demonstrate that with certain modification the acid vapor gas phase functionalization can be successfully applied in the case of thinner (6–7nm) densely aligned millimetre high CNTs at the same time preserving the morphology. Reactor simplicity, ambient pressure and low temperature operation make this method very promising for application in CNT gas-phase functionalization with oxygen containing functional groups (mainly carboxyl and hydroxyl).

### **9.1. Experimental setup**

For performing of gas phase functionalization of CNT appropriate reactor was made. Heater – the most important part of the reactor was made of a glass tube with appropriate welded necks and exhaust connection. Nickel chrome wire was coiled around the tube and quartz wool was applied as heat isolation. Temperature was calibrated by a K-type thermopar inserted inside the tube and controlled by a direct current power source.

Schematic setup is presented at Figure 33. Nitric acid vapor was produced from concentrated liquid nitric acid (heated to near boiling temperature) inside of the two-neck flask. The vapor passes through the heating zone of the reactor and is directed further to the condenser where the vapor condenses and is collected. The setup prevents condensation of the acid vapor onto CNTs and thus the functionalization takes place fully under gas-phase conditions. The heating zone temperatures were varied from 125°C to 200°C and the treatment times from 1 to 14 hours.

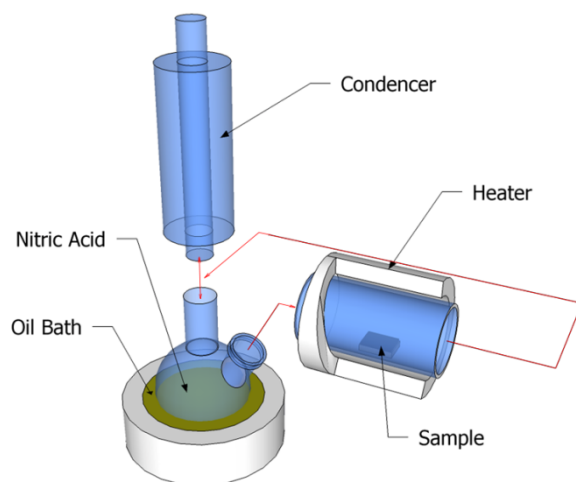


**Figure 33.** Schematic of the reactor set-up for gas-phase functionalization of CNTs with nitric acid.

## 9.2. Results and Discussion.

It is well known that the functionalization process depends from certain parameters like a choice of an oxidizing agent, its concentration, an environment, reaction temperature and duration, etc. Nitric acid, which was also used in our study, is a well-known reagent for CNT functionalization and is one of the most promising reagents for many technologies. Ambient atmosphere significantly lowers the cost of the process making it much easier and more efficient. One of the major advantages of this method is that the samples can be taken out and inspected at any moment, so the functionalization dynamics can be observed and desirable degree of functionalization can be achieved.

Note however, that there are certain limitations of the process parameters. For instance, using temperatures below 125°C are not possible due to the boiling point of the zoetrope (below 125°C acid vapor will condensate on the sample and heater walls). At temperatures higher than 200°C a fast destruction of the morphology of the aligned nanotubes was observed. For optimal results the reaction times and temperatures should be optimized keeping in mind that these strongly depend on diameter, density and quality (i.e. density and location of defects) of CNTs. Nanotubes with smaller diameter are more reactive, due to larger sidewall curvature, and also have smaller number of walls (which in case of defects propagation leads to cutting of CNTs).

For most application of covalently functionalized CNTs the sidewall functionalization is the most important. And for investigation of its functionalization dynamics the data from oxygen to carbon ratio from EDS measurements were used. The spectra were collected from the side region of the ACNT where no

interfering signal from substrate oxide was present. It is reasonable to assume that all oxygen signal that was observed in the spectra belongs to the functional groups. Moreover, the nanotubes' ends were also not included. Figure 34 shows a dependence of oxygen to carbon ratio from the reaction temperature and time obtained from the EDS measurements. Figure 35 shows ACNT after the treatment at different temperatures.

At higher temperatures the acid vapor reacts more aggressively, causing not only the functionalization but also a cutting of CNTs from the substrate (Figure 35, at 175°C and 200°C). Note that the latter preferably happens in defect-rich regions of CNTs. In certain cases the CNTs grown in the thermal CVD reactor can be less regular at the both ends of the tubes, therefore at high temperatures the treatment can lead to complete cutting off of the ACNTs from a substrate (Figure 36).

However, when the concentration of defects in the near-substrate region is lower, excessive acid treatment results in a different destruction of the CNTs' morphology (Figure 37).

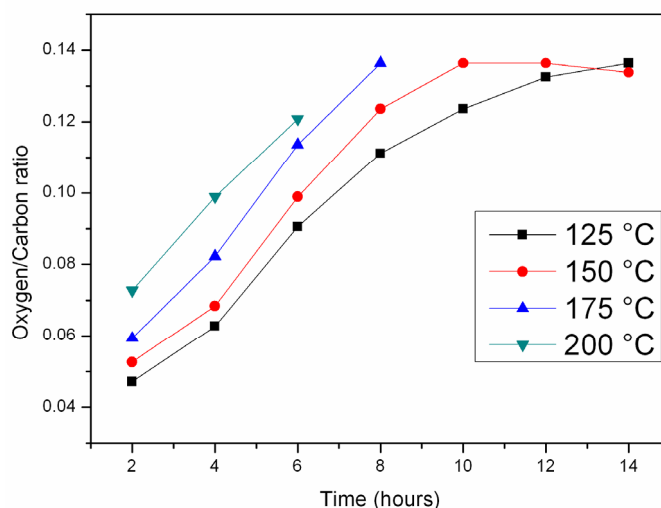


**Figure 34.** Oxygen to carbon ratio of the ACNTs side walls as a function of the reaction temperature (°C) and time (hours) obtained from EDS measurements. Note that at higher temperatures the morphology of the samples can be preserved for shorter times.

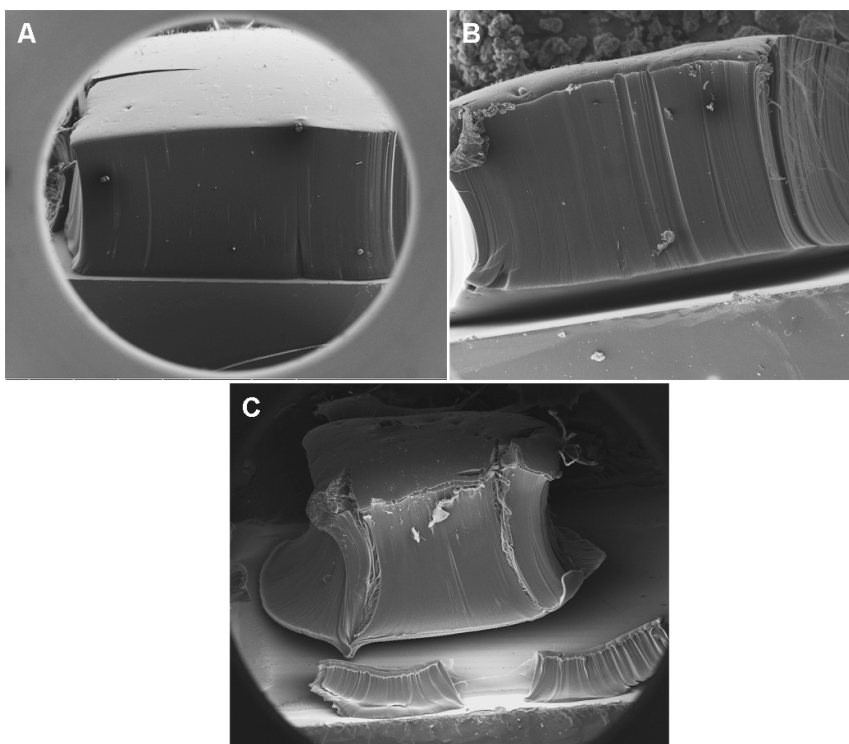


**Figure 35.** ACNT after 4 hours treatment with nitric acid vapor at a) 125°C b) 175°C and c) 200°C

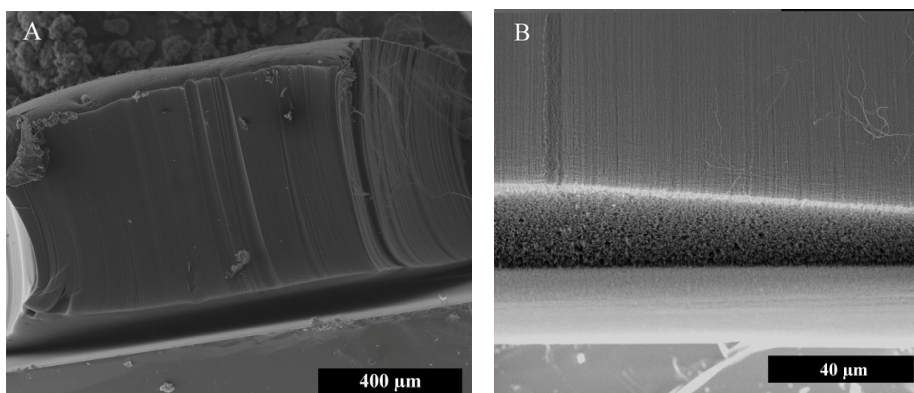


**Figure 36.** SEM images of the side view of a) ACNT treated in nitric acid vapor for 1 hour at 200°C b) cut-off region at higher magnification.

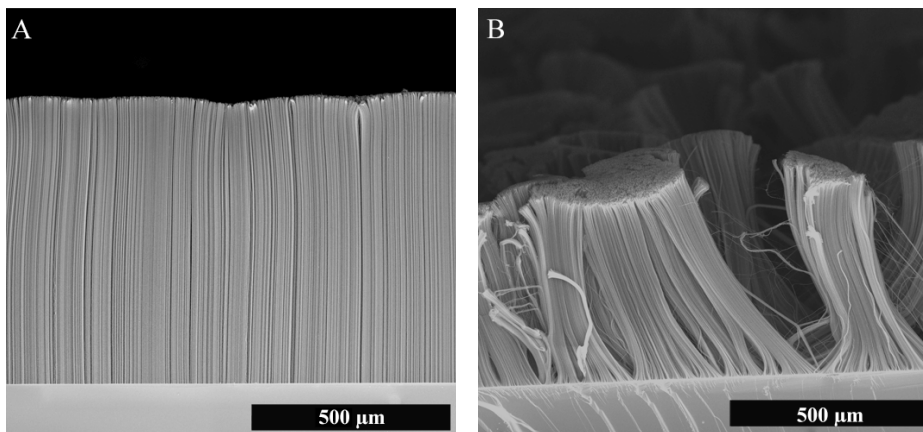


**Figure 37.** SEM images of the side view of vertically ACNTs a) before acid vapor treatment b) the same sample after 3 hours of treatment at 200°C.

The morphology is substantially altered by creation of randomly distributed defects distorting thus the orientation while keeping most of the CNTs attached to the surface (Figure 37b). In order to maintain initial well-aligned structure of CNTs, temperatures between 125–150°C should be applied. At these temperatures functionalization process is slower, less aggressive, and leads to formation of desirable concentration of oxygen containing groups without destroying the morphology (Figure 38).

For verification of the uniform functionalization of the ACNTs throughout a sample, some samples were randomly fractured after the final step of the treatment and studied inside the “forest” of the ACNT. No deviation of the results was observed confirming the uniform diffusion of the vapor throughout the sample.

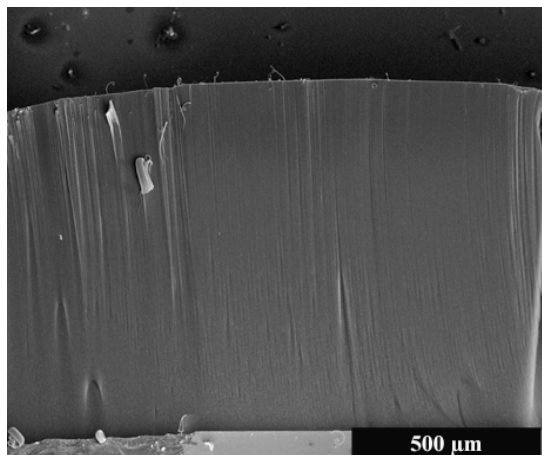


**Figure 38.** SEM side-view of the ACNT sample functionalized at 125°C for 12h.



For characterization of the samples series of Raman, FT-IR, EDS, and XPS analysis were performed.

Raman spectroscopy is very useful tool in analyzing the graphitization degree of carbon-based materials. Different  $I_D/I_G$  ratios of the samples illustrate different crystalline structure. As synthesized CNT had the  $I_D/I_G$  ratio 0.87 and CNTs functionalized for 10 hours in nitric acid vapor at 150°C had the ratio 1.38. Increased  $I_D/I_G$  ratio of the functionalized ACNT can be attributed to chemical oxidation that partially disrupts CNT structure (more details about Raman and FT-IR spectra in Paper V).

XPS is widely used method for determination of functional groups linked to CNTs. However, XPS is rather complicated, time-consuming and expensive method. The main problem with XPS of the functionalized ACNTs however, is related to large excitation area necessary for XPS measurements, which means that the sidewalls of ACNTs could not be directly measured using as grown ACNTs. To make larger samples the CNTs were first dispersed in ethanol and then placed on a cleaned silicon substrate to achieve homogeneous distribution that would represent the whole sample. Note that the spectra measured with a configuration where the x-ray beam is parallel to ACNT tends to strongly overestimate the oxygen-to-carbon ratio because the signal is generated mainly from the apexes of the CNTs where the concentration of the defects can be significantly higher.

In Figure 39, C 1s XPS spectrum of untreated CNTs (Figure 39a) and treated in nitric acid vapour for 10 hours at 150°C is shown (Figure 39b). The spectra were analyzed using the procedure described in [104]. The broad C 1s peak ranging from 282 to 294 eV in the XPS spectra consists of peaks attributed to several carbon-based functional groups that have different binding energies. The main peak at 284.3 eV can be assigned to the  $sp^2$ -hybridized graphite-like carbon. C 1s peak was fitted using Gaussian-Lorentzian hybrid function. A good fit was achieved with six separate peaks, each representing differently bound carbon:  $sp^2$  at 284.3 eV,  $sp^3$  at 285.2 eV, -C-O- at 286.5 eV, -COO- at 288.5 eV, carbonate at 290.2 eV and  $\pi-\pi^*$  at 291.8 eV [105]. As can be clearly seen from Figure 39b, nitric acid oxidation increases the intensity of  $sp^3$  and -COO- related peaks.

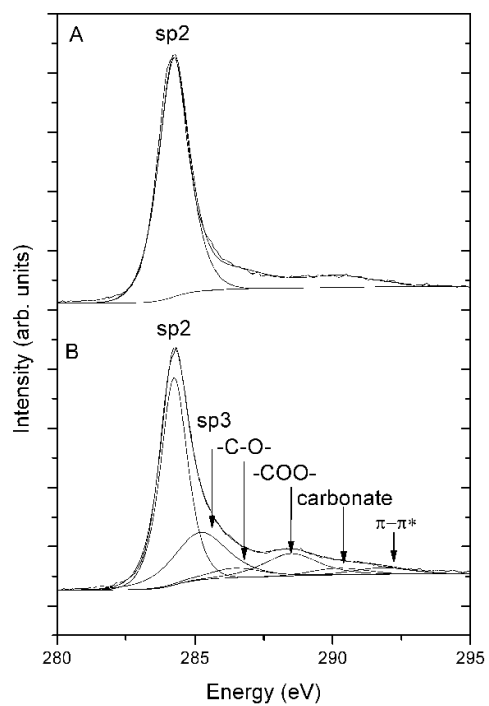


**Figure 39.** XPS spectra of C 1s a) untreated CNTs and b) treated in nitric acid vapour for 10 hours at 150°C.

## 10. FORMATION OF NICKEL OXIDE NANOSTRUCTURES ON TiO<sub>2</sub> (Paper – II)

In this work we present an alternative approach for preparation NiO nanostructures that can be used as catalysts for growing CNT's. We investigated the formation of NiO nanostructures during sol-gel process that is relatively simple, cost-effective and readily applicable method for preparation several oxide materials and different structures [106]. Our approach harnesses intrinsic self-assembling of precursor materials, and in contrast to above-mentioned method by Huang is therefore applicable over unlimited surface area and also in cases of complicated structures (for example described in paper III).

Nickel doped thin films were prepared by sol-gel method using commercially available titanium (IV) butoxide and nickel (II) nitrate hexahydrate (dopant) as the starting materials. For the film deposition 23.3% polymeric precursor solution in hexane was prepared. Thin films were prepared by dropping (from height of 5 mm) the precursor solution droplet (3 mg) onto monodistilled water surface at 21°C. The precursor polymerized rapidly and a floating thin film was formed on water surface. The films were collected on mica substrate by dropping the water level until the substrate surfaced and captured the film. Before heat treatment the obtained thin films were kept at room temperature in air for 24 hours. To release the remaining organic solvents and to crystalline the material, the films were baked in an oven (in air) raising the temperature to 700°C within 4h and keeping at the temperature from 1 to 10 h.

Before and after heat treatment the samples were analyzed with XPS. XPS confirmed absence of nickel before and its appearance after the heat treatment. Even the shortest baking time of the samples caused drastic appearance of Ni lines in the spectra. The relative intensity of Ni lines gradually increased as the baking time was increased.

Topography of the samples was analyzed by AFM (Figure 40).

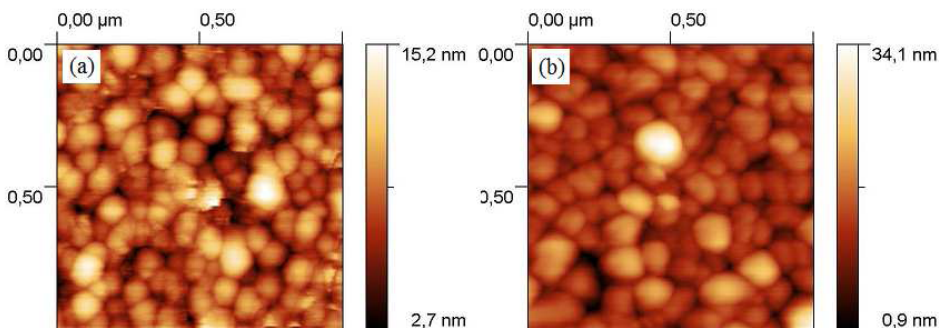


**Figure 40.** a) AFM topographic image of the sample heated for 1h at 700°C. (b) AFM topographic image of the sample heated for 10 h at 700°C.

Detailed analysis of the AFM images supported the result of the XPS measurements that concentration of the surface Ni was increased as the result of the heating.

Later some CNT growth experiments were performed on these samples. Results confirmed that nickel concentrates on the surface in the form of nanoparticles, which diameters depend on nickel concentration, treatment time and temperature (Figure 41)

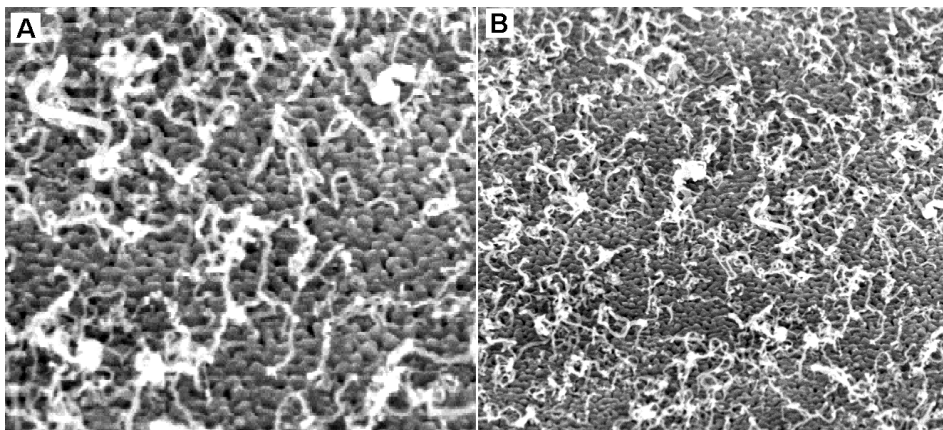


**Figure 41.** Electron microscope image of heated Ni doped  $\text{TiO}_2$  thin film on  $\text{SiO}_2$  after CNT synthesis a) close up image b) larger area image.

## **II. PREPARATION OF STRUCTURED SOL-GEL FILMS USING TAPE CASTING METHOD (Paper – III)**

Various sol–gel coatings are well-known and widely used in many technologies [107]. Their application in the field of CNT growth offer simple preparation process, no need for complicated apparatus and availability to form substrate in variety of forms (thin films, fibers, micro and nanoparticles etc.). For different applications several methods for preparation of sol–gel films have been developed: spin coating, dip coating, spray coating, silk screen printing, etc. (see, e.g. review papers [108] and [109] and references therein). However, none of forementioned methods is universal and while being optimized for a certain application they lack performance in another. For example, all of these processes utilize highly diluted and therefore low viscosity precursor. The latter in turn often restricts formation of thick and/or structured coatings. Therefore, there is an active search for new methods which would open new possibilities for preparing sol–gel films.

Tape casting (also called doctor's blade method) is an industrial scale method, where a slurry is casted onto a substrate through a slit between the substrate and a blade. A film is produced which thickness is determined by the width of the slit. And easy variation of the method could be a big advantage for application in the field of CNT synthesis. For instance, if the method described in Paper III is used for producing catalytic particles for the CNT synthesis, the film thickness often determines nanoparticles distance from possible “poisoning” substrate material extending thus their activity period. Moreover, the film thickness also influences the amount and density of catalytical nanoparticles. Suitable slurries are generally multicomponent mixtures of ceramic powders, solvents, plasticizers, and binders. The nature of the slurries is very different compared to homogeneous sols used in sol–gel chemistry. However, it is interesting to note, that ceramic powders as one components of slurries are sometimes prepared by sol–gel methods (see, e.g. [110] and [111]). Smearability and preservation of their geometrical shape after the coating are requirements for slurries in the tape casting.

In the present work, we demonstrate that molecular level homogeneous high viscosity sol–gel precursors can be used instead of slurries to prepare surface coatings by the tape casting method. It is important to note that sol–gel precursors used in the present work are not mixtures of different constituents, but homogeneous oligomer concentrates (known also as oligomeric/polymeric melts). Consequently nanometer level smoothness is possible in contrast to slurries, which smoothness is limited by the sizes of the ceramic particles restricting thus their application in nanotechnology.

Figure 42 shows the principle scheme of the tape casting machine. The sample holder is fixed onto the linear translation stage, which is driven from one side by a servo motor and stabilized from other side with two springs. Above the linear translation stage there is located a blade, which is pressed against the substrate. A high viscosity sol is directed to the moving substrate behind the immobile blade that smears the sol onto the substrate. The speed of the linear motion, blade pressure and the angle between the blade and the substrate can be varied. It is also possible to use either sharp and uniform, or structured blades from different materials.

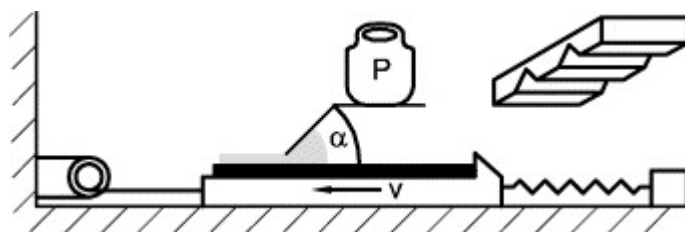


**Figure 42.** Working principle of the tape casting machine. Substrate is driven with speed  $V$ , on the immobile blade is applied pressure  $P$  and angle between the blade and the substrate is  $\alpha$ . Substrate is black and sol is marked with grey. Inset on the right demonstrates the shape of structured blade.

The film formation process is a complex phenomenon consisting of several sub-processes acting at different time and length scales and affecting the process frequently in opposite directions. Naturally, also the sol's intrinsic properties such as viscosity should be counted. The higher the viscosity, the faster the gelation takes place and the smaller are distortions of smeared structures caused by capillary forces and by mass loss during gelation. If gelation is too fast and sample thickness is too large, cracks appear.

Figure 43 clearly demonstrate that tape casting method can successfully be applied for production of well-defined linear structures. The overall resemblance of formed structures to the blade is good, e.g. the structure's periodicity is very close to the blade's one. It means that horizontal shrinkage of the structures during gelation process is almost negligible, since formed structures are strongly connected with the substrate. Note however, that in the shown example, the shape of a groove is not identical replica of the blade's structure and the shrinkage of the structures in vertical direction during the gelation process is up to four times.

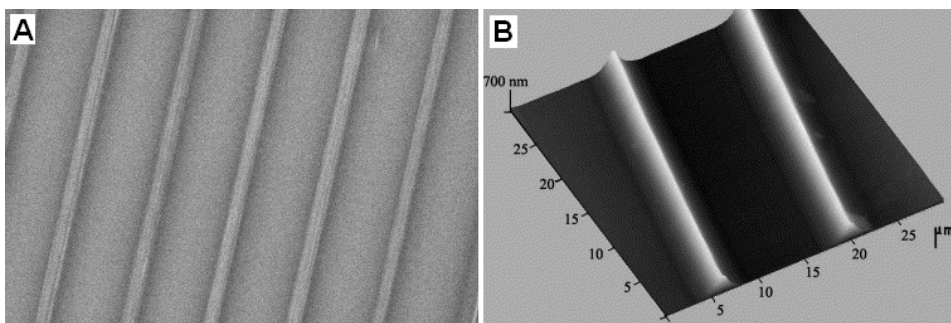


**Figure 43.** Image of tape casted microstructure film obtained by a) SEM and b) AFM

## 12. METHOD OF CLEANING THE TIP OF ATOMIC FORCE MICROSCOPY (Patent IV)

AFM is widely used tool for surface characterisation and can be used for nanoparticles and nanotubes characterisation on a surface. However, the latter can often lead to probe contamination with adhered materials, which can cause several problems. AFM tips are quite expensive, sometimes unique custom made tips are used, and replacement of the tip can lead to losing the particular site of interest and its time consuming relocation. We have developed a method, which is capable of cleaning the tip *in situ* without taking AFM cantilever out or moving it from its position relative to the substrate. The cleaning of the AFM tip is performed directly in the place of the measurement. The method is based on the idea that a cleaning agent is condensed directly to the examined object, for example, in the form of carbon dioxide snow. The possible scheme of the setup for the cleaning is shown in Figure 44. Carbon dioxide snow is deposited on the sample and by scanning the tip over the surface the contaminants are removed from the tip due to abrasive properties of the snow.

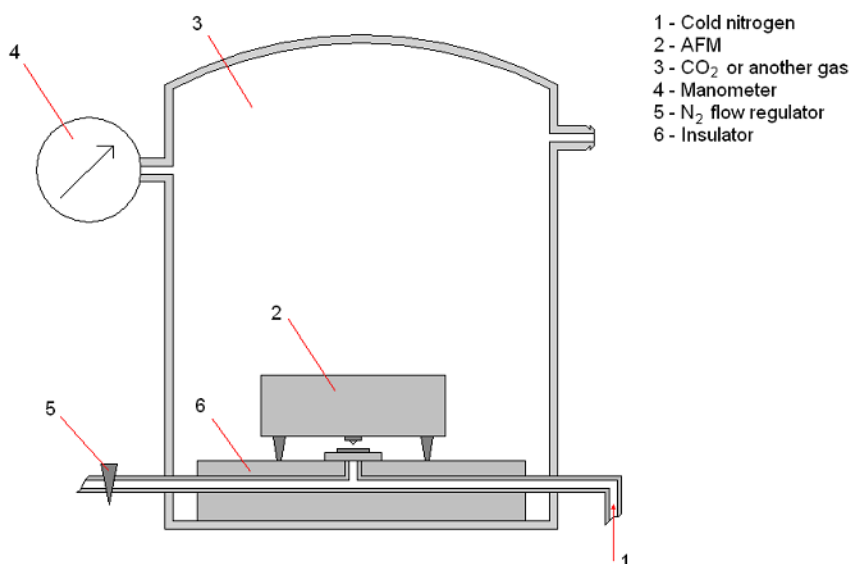
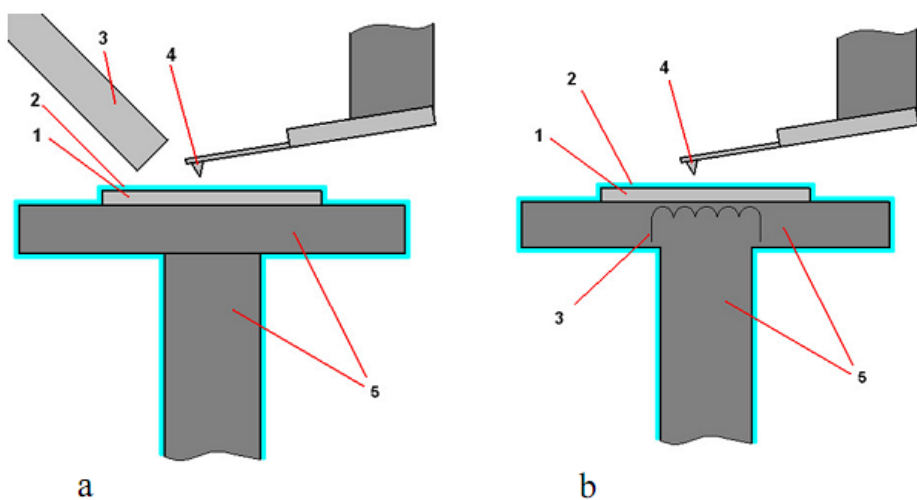


**Figure 44.** Setup for cleaning of AFM tips

After the cleaning scan cycle the tip is heated quickly and the cleaning agent is vaporized together with contaminants (Figure 45). Cleaning in such way enables to continue measurements from the same position on the substrate where it was interrupted because of the contamination.





- 1 – Sample
- 2 – CO<sub>2</sub> snow or other condensed gas
- 3 – Light guide or local heating
- 4 – AFM tip
- 5 – Cold Finger

**Figure 45.** After the cleaning scan cycle the tip is heated locally either by light guide (a) or electrically (b).

## SUMMARY AND CONCLUSION

The research compiled into the present thesis deals with several aspects of experimental investigation of synthesis of carbon nanotubes (CNT) that can lead to development of different industrial technologies. Within the framework of this thesis several original catalytical systems for CNT synthesis were developed, which include a simple and versatile method for potential mass-production of CNTs, a method for growing well-oriented CNTs and a method for growing CNTs on complicated structures based on sol-gel technology. For the bulk growth of CNTs the method is based on the self-assembling of cobalt nanoparticles on aluminium substrate during evaporation of Al and Co salts solution. The developed method for synthesis of aligned CNTs enable growing CNTs up to several millimetres. Their subsequent treatment with nitric acid vapor in the original gas phase functionalization reactor under ambient conditions results in functionalised CNTs without altering their morphology. Uniform functionalization of the densely aligned CNT forests demonstrated the possibility to apply the process in large-scale treatment of the nanotubes.

Also, a method for doping aligned CNTs with nitrogen was developed and its potential application was demonstrated in the case of fuel cell technology by synthesizing electrochemically highly active vertically aligned nitrogen doped CNTs on glassy carbon electrodes for oxygen reduction reactions.

In addition, several thin film layer catalyst systems described in the literature were further investigated, adopted and modified for utilization in our original reactors. Several CVD reactors were constructed and modified for particular synthesis conditions (cold wall, hot wall and their modifications) that gave possibility to grow and investigate very different CNTs.

Additionally, modifications of CNT characterization techniques were performed, namely, an original method for *in situ* atomic force microscope (AFM) tip cleaning was developed and patented. The method used abrasive properties of carbon dioxide snow and one of its major advantages was cleaning the tip *in situ* without repositioning of AFM or removing the tip.

## SUMMARY IN ESTONIAN

### Nanostruktuuride interaktsioon ja iseorganiseerumine

Käesolev uurimistöö on seotud eeskätt süsinik-nanotorude kasvatusmeetodite väljatöötamisega ja nanotorude omaduste uurimisega. Töö peamiseks tulemuseks on mitmete originaalsete katalüsaatorsüsteemide väljatöötamine ja nende rakendatavuse uurimine. Üks väljatöötatud meetod baseerub sool-geel meetodil valmistatud maatriksmaterjalist lisandmetalli difusiooni tulemusena katalüsaatorosakeste formeerimises maatriksi pinnal, mis võimaldab nanotorusid kasvatada keeruliste 3D mikrostruktuuride sise- ja välispindadele.

Töötati välja lihtne ja efektiivne meetod süsinik-nanotorude kasvatamiseks, mis baseerub Al pinnal Co nanoosakeste iseorganiseerumisel Al ja Co soolade lahuse aurustumisel. Meetod on eeskätt suunatud rakendamiseks tööstuslikus tootmises.

Töötati välja meetod orienteeritud süsinik-nanotorude kasvatamiseks ning nende funktsionaliseerimiseks lämmastiku ja muude keemiliste rühmadega eesmärgiga rakendada orienteeritud süsinik-nanotorude struktuure erinevates peamiselt enereetikaga seotud rakendustes (näit. kütuseelementide elektroodid jms.)

Katsete läbiviimiseks ja meetodikate väljatöötamiseks valmistati mitmed keemilise aursadestuse reaktorid, muuhulgas nii külma- kui ka kuumaseinalist tüüpi ning nende modifikatsioone. Juurutati ja modifitseeriti mitmeid kirjanduses avaldatud süsinik-nanotorude kasvatamise meetodeid eesmärgiga leida sobivaimad lahendused väljatöötatud seadmete jaoks.

Osaliselt käesoleva uurimistöö läbiviimiseks töötati välja ja patenteeriti meetod teravikmikroskoopia sensori puhastamiseks.

## REFERENCES

1. Ruelle B. Functionalization of carbon nanotubes via plasma post-discharge surface treatment: Implication as nanofiller in polymeric matrices. *Laboratoire de Chimie Inorganique et Analytique*. 2009.
2. Radushkevish L.V., Lukyanovich V.M., *Zurn. Fisic. Chim.*, 1952, 26, 88–95
3. Hillert M., Lange L., *Z Kristallogr*, 1958, 111, 24–34
4. Baker R.T.K., Harris P.S., Thomas R.B., Waite R.J., *J Catal.*, 1973, 30, 86–95
5. Oberlin A., Endo M., Koyama T., *J Cryst. Growth.*, 1976, 32, 335–349
6. Kroto H.W., Heath R. J., O'Brien S. C., Curl R.F., Smalley R.E., *Nature*, 1985, 318, 162
7. Iijima S., *Nature* 1991, 354, 56–58
8. Iijima S., Ichihashi T., *Nature* 1993, 363, 603–605
9. Bethune D.S., Klang C.H., de Vries M.S., Gorman G., Savoy R., Vazquez J., Beyers R., *Nature* 1993, 363, 605–607
10. Saito R., Dresselhaus G., Dresselhaus M. S. *Physial Properties of Carbon Nano-tubes*. London: Imperial College Press, 1998
11. Dresselhaus M.S., Dresselhaus G., Eklund P.C. *Science of fullerenes and carbon nanotubes*. Academic Press, San Diego, California, 1996
12. Dommele S. Nitrogen containing CNT, synthesis, characterization and catalysis. *Universiteit Utrecht*, 2008
13. Belin T., Epron F., *Mater. Sci. Eng.* 2005, B119, 105–118
14. Thostenson E.T., Ren Z., Chou T.-W., *Compos. Sci. Technol.* 2001, 61, 1899–191
15. [www.cobweb.ecn.purdue.edu](http://www.cobweb.ecn.purdue.edu), 2009–06
16. Saito R., Fujita M., Dresselhaus G., Dresselhaus M., *Appl. Phys. Lett.*, 1992, 60, 2204–2206
17. Yakobson B.I., Brabec C.J., Bernholc J., *Phys. Rev. Lett.* 1996, 76(14), 2511–251
18. Yi J.Y., Bernholc J. *Phys. Rev. B*, 1993, 47, 1708–1711
19. Ewels C. P., Glerup M., *J. Nanosci. Nanotech.*, 2005, 5, 1345–1363
20. Czerw R., *et al.*, *Nanoletters*, 2001, 1(9), 457–460
21. Hellgren N., Johansson M.P., Broitman E., Hultman L., Sundgren J-E., *Phys. Rev. B*, 1999, 59, 5162–5169
22. Ronning C., Feldermann H., R. Merk, H. Hofsäss, P. Reinke, J.-U. Thiele, *Phys. Rev. B*, 1998, 58 (4), 2207–2215
23. Kim S.Y., Lee J., Na C. W., Park J., Seo K., Kim B., *Chem. Phys. Lett.*, 2005, 413, 300–305
24. Choi H, Ihm J, Louie S, Cohen M., *Phys. Rev. Lett.*, 2000, 84, 2917–20
25. Liu X, Pichler T, Knupfer M, Fink J, Kataura H., *Phys Rev B* 2004, 70, 205405–205610
26. Ma J, Guan S, Lai CH. *Phys Rev B.*, 2006, 74, 205401–205406
27. Stephan O, Ajayan P., *Science*, 1994, 266, 1863–1865
28. Raymundo-Pinero E., Cazorla-Amoros D., Linares-Solano A., Find J., Wild U., Schlogl R., *Carbon*, 2002, 40, 597–608
29. Pels J.R., Kapteijn F., Moulijn J.A., Zhu Q., Thomas K.M., *Carbon*, 1995, 33(11), 1641–1653
30. Dommele S., Jong K.P., Bitter J.H., *Chem. Commun.*, 2006, 4859–4861
31. Dommele S., Romero-Izquierdo A., Brydson R., Jong K. P., Bitter J. H., *Carbon*, 2008, 46, 138–148

32. Journet C., Bernier P., Appl. Phys. A-Mater. Sci. & Proces., 1998, 67(1), 1–9
33. Journet C., Maser W.K., Bernier P., Loiseau A., delaChapelle M. L., Lefrant S., Deniard P., Lee R., Fischer J.E., Nature, 1997, 388 (6644), 756–758
34. Harris P.J.F., Carbon nanotubes and related structures – New materials for the twenty-first century. Cambridge University Press, Cambridge, UK, 1999
35. Teo K.B.K., Singh Ch., Chhowalla M., Milne W.I. Catalytic synthesis of carbon nanotubes and nanofibers. In Encyclopedia of Nanoscience and Nanotechnology; Nalwa, H.S., Ed.; American Scientific Publisher: Valencia, CA, USA, 2003, Vol 1, pp. 665–668
36. Seo J.W., Magrez A., Milas M., Lee K., Lukovac V., Forro L., J. Phys. D: Appl. Phys., 2007, 40, 109–120
37. Szabo A., Perri C., Csato A., Giordano G., Vuono D., Nagy J. B., Materials, 2010, 3, 3092–3140
38. Ren Z.F., Huang Z.P., Xu J.W., Wang J.H., Bush P., Siegal M.P., *et al.* Science, 1998, 282, 1105
39. Hafner J.H., Bronikowski M.J., Azamian B.R., Nikolaev P., Rinzler A.G., Colbert D.T., Smith K.A., Smalley R.E., Chem. Phys. Lett., 1998, 296, 195–202
40. Fan S.S., Chapline M.G., Franklin N.R., Tomblor T.W., Cassell A.M., Dai H., Science, 1999, 283, 512–514
41. Nessim G. D., Matteo S., Desire'e L. Plata, Kevin P. O'Brien, Hart A. J, Eric R. Meshot, Reddy C.M., Gschwend P. M., Thompson C. V., Carbon, 2011, 49, 804–810
42. Kumar M., Ando Y., Nanosci. J. Nanotechnol., 2010, 10, 3739–3758
43. Baker R. T. K., Barber M. A., Harris P. S., Feates F. S., Waite R. J., J. Catalysis, 1972, 26, 51–60
44. Baker R.T. K. and Waite R. J., J. Catalysis, 1975, 37, 101–105
45. Sinnott S. B., Andrews R., Qian D., Rao A. M., Mao Z., Dickey E. C., and Derbyshire F., Chem. Phys. Lett., 1999, 315, 25–29
46. Li J., Vergne M.J., Mowles E.D., Zhong W-H, Hercules D.M., Lukehart C.M., Carbon, 2005, 43, 2883–2893
47. Konyushenko E. N. *et al.*, Polymer, 2006, 47, 5715–5723
48. Ramanathan T., Fisher F.T., Ruoff R.S., Brinson L.C., Chem. Mater., 2005, 17, 1290–1295
49. Choi H.C., Park J., Kim B., Phys J. Chem. B, 2005, 109, 4333–4340
50. Lee Y.T., Kim N.S., Park J., Han J. B., Choi Y.S., Ryu H., Lee H.J., Chem. Phys. Lett., 2003, 372, 853–859
51. Terrones M. *et al.*, Adv. Mater., 1999, 11 (8), 655–658
52. Tang C., Bando Y., Goldberg D., Xu F., Carbon, 2004, 42, 2625–2633
53. Liu G., Li X., Ganesan P., Popov B. N., Electrochimica Acta, 2010, 55, 2853–2858
54. Kundu S., Nagaiah T. C., Xia W., Wang Y., Dommele S. V., Bitter J. H., Santa M., Grundmeier G., Bron M., Schuhmann W., Muhler M., J. Phys. Chem. C, 2009, 113, 14302–14310
55. O'Connell M. J., Boul P., Ericson L. M., Huffman C., Wang Y.H., Haroz E., Kuper C., Tour J., Ausman K.D., Smalley R.E., Chem. Phys. Lett., 2001, 342, 265–271
56. Bayazit M. K., Clarke L. S., Coleman K. S., Clarke N., J. Am. Chem. Soc., 2010, 132, 15814–15819
57. Suri A., Chakraborty A. K., Coleman K. S., Chem. Materials, 2008, 20, 1705–1709
58. Hirsch A., Angewandte Chemie-International Edition, 2002, 41, 1853–1859

59. Banerjee S., Kahn M. G. C., Wong S. S., *Chemistry-A European Journal*, 2003, 9, 1899–1908
60. Tasis D., Tagmatarchis N., Bianco A., Prato M., *Chem. Rev.*, 2006, 106, 1105–1136
61. Niyogi S., Hamon M. A., Hu H., Zhao B., Bhowmik P., Sen R., Itkis M. E., Haddon R. C., *Accounts Chem. Res.*, 2002, 35, 1105–1113
62. Bahr J. L., Tour J. M., *J. Mat. Chem.*, 2002, 12, 1952–1958
63. Tasis D., Tagmatarchis N., Georgakilas V., Prato M., *Chem. Eur. J.*, 2003, 4000–4008
64. Liu J., Rinzler A. G., Dai H. J., Hafner J. H., Bradley R. K., Boul, P. J., Lu, A., Iverson T., Shelimov K., Huffman C. B., Rodriguez-Macias F., Shon, Y. S., Lee T. R., Colbert D. T., Smalley R. E., *Science*, 1998, 280, 1253–1256
65. Duesberg G. S., Burghard M., Muster J., Philipp G., Roth S., *Chem. Comm.*, 1998, 435–436
66. Islam M. F., Rojas E., Bergey D. M., Johnson A. T., Yodh A. G., *Nano Lett.*, 2003, 3, 269–273
67. Bandow S., Rao A. M., Williams K. A., Thess A., Smalley R. E., Eklund P. C. J. *Phys. Chem. B.*, 1997, 101, 8839–8842
68. Tsang S. C., Guo Z. J., Chen Y. K., Green M. L. H., Hill H. A. O., Hambley T. W., Sadler P. J., *Angewandte Chemie-International Edition in English*, 1997, 36, 2198–2200
69. Hu H., Bhowmik P., Zhao B., Hamon M. A., Itkis M. E., Haddon R. C., *Chem. Phys. Lett.*, 2001, 345, 25–28
70. Sinnott S. B., *J. Nanosci. Nanotechnol.* 2002, 2, 113–123
71. Charlier J.-C., *Acc. Chem. Res.* 2002, 35, 1063–1069
72. Chen J., Hamon M. A., Hu H., Chen Y., Rao A. M., Eklund P. C., Haddon R. C., *Science*, 1998, 282, 95–98
73. Zhang J., Zou H., Qing Q., Yang Y., Li Q., Liu Z., Guo X., Du Z., *J. Phys. Chem. B.*, 2003, 107, 3712–3718
74. Chen Z., Thiel W., Hirsch A., *Chem. Phys. Chem.*, 2003, 4, 93–97
75. Haddon R. C., *Acc. Chem. Res.*, 1998, 21, 243–249
76. Hamon M. A., Itkis M. E., Niyogi S., Alvarez T., Kuper C., Menon M., Haddon R. C., *J. Am. Chem. Soc.* 2001, 123, 11292–11293
77. Balasubramanian K., Burghard M., *Small* 2005, 1, 180–192
78. Fu K. F., Huang W. J., Lin Y., Riddle L. A., Carroll D. L., Sun Y. P. *Nano Letters*, 2001, 1, 439–441
79. Wong S. S., Joselevich E., Woolley A. T., Cheung C. L., Lieber C. M., *Nature*, 1998, 394, 52–55
80. Hamon M. A., Hui H., Bhowmik P., Itkis H. M. E., Haddon R. C., *Appl. Phys. Materials Sci. Proc.*, 2002, 74, 333–338
81. Monthieux M., Smith B. W., Burteaux B., Claye A., Fischer J. E., Luzzi D. E., *Carbon*, 2001, 39, 1251–1272
82. Konya Z., Vesselenyi I., Niesz K., Kukovecz A., Demortier A., Fonseca A., Delhalle J., Mekhalif Z., Nagy J. B., Koos A. A., Osvath Z., Kocsanya A., Biro L. P., Kiricsi I., *Chem. Phys. Lett.*, 2002, 360, 429–435
83. Ma P. C., Tang B. Z., Kim J.-K., *Chem. Phys. Lett.* 2008, 458, 166–169
84. Byl O., Liu J., Yates J. T. *Langmuir*, 2005, 21, 4200–4204
85. Bubert H., Brandl W., Kittel S., Marginean G., Toma D., *Anal. Bioanal. Chem.*, 2002, 374, 1237–1241

86. Hou P. X., Liu C., Cheng H. M., Carbon, 2008, 46, 2003–2025
87. Xia W., Jin C., Kundu S., Muhler M., Carbon, 2009, 47, 919–922
88. <http://mse.iastate.edu/microscopy/whatsem.html>
89. Hayak M.A, Principles and Techniques of Scanning Electron Microscopy, Van Nostrand Reinhold Co., 1978
90. Zhou W., Apkarian R.P., Wang Z.L., Joy D. “Fundamentals of Scanning Electron Microscopy (SEM) in Zhou, Weilie”, Scanning Microscopy for Nanotechnology: Techniques and Applications, Springer, New York, 2007
91. Scanning electron microscope. [Art]. In Encyclopædia Britannica. Retrieved from <http://www.britannica.com/EBchecked/media/110970/Scanning-electron-microscope>
92. Peterson B. P. Energy Dispersive Spectroscopy Characterization of Solute Segregation in Ti-6Al-4V. Ohio State University. 2011
93. Kemal B. M., Synthesis and Properties of Chemically Modified Carbon Nanotubes. Durham University. 2010.
94. Briggs D. and Seah M. P., Practical Surface Analysis by Auger and X-Ray photoelectron Spectroscopy, Eds. New York: Wiley, 1983
95. Spectroscopy Volume Three; Straughan, B. P., Walker S., Eds.; Chapman and Hall: London, 1976
96. Ayala P., Grüneis A., Kramberger C., Rummeli M. H., Solórzano I. G., Freire F. L., Pichler T., Chem J. Phys., 2007, 127, 184709–184716
97. Yang Z., Xia Y., Mokaya R., Chem. Mater., 2005, 17, 4502–4508
98. Lee D.H., Lee W.J., Kim S.O., Nano Lett., 2009, 9, 1427–1432
99. Nguyen C. V., Delzeit L., Cassell A. M., Li J., Han J., Meyyappan M., Nano Lett., 2002, 2, 1079–1081
100. Chen Q. D., Dai L. M., Gao M., Huang S. M., Mau A., J. Phys. Chem. B, 2001, 105, 618–622
101. Hinds B. J., Chopra N., Rantell T., Andrews R., Gavalas V., Bachas L. G., Science, 2004, 303, 62–65
102. See paper I
103. Datsyuk V., Kalyva M., Papagelis K., Parthenios J., Tasis D., Siokou A., Kallitsis I., Galiotis C., Carbon, 2008, 46, 833–840
104. Sakka S, Kozuka H (editors) 2005 Handbook of sol-gel science and technology: processing, characterization and applications. Volume I, Sol-gel processing, Kluwer Academic Publishers.
105. Attia S.M., Wang J., Wu G. M., Shen J., Ma J. H., J. Mater. Sci. Technol. 2002, 18, 211–215
106. Brinker C.J. and Scherer G.W., Sol–Gel Science, Academic Press, San Diego 1990
107. Brinker C. J., Hurd A. J., Schunk P. R., Frye G. C. and Ashley C.S. J. Non-Cryst. Solids, 1992, 424, 147–148
108. Sacca A., Carbone A., Passalacqua E., D’Epifanio A., Licoccia S., Traversa E., Sala E., Traini F., Ornelas R., J. Power Sources, 2005, 152, 16–22
109. Sharma P. K., Varadan V. V., Varadan V. K., Smart Mater. Struct., 2003, 12, 749–754

## ACKNOWLEDGEMENTS

First of all I would like to thank my supervisor Ilmar Kink for involving and continuously supporting me in such an interesting research, and especially for some critics and advises concerning new ideas.

I thank also colleagues especially Ants Lõhmus for his patients and help with designing new instruments and set-ups; Alexey Treshchalov for collaboration in synthesis of millimeter scale ACNT; Sergei Tsarenko for performing synthesis of ACNT and technical side of the synthesis; Vladimir Tsubin for cold-wall reactor construction and help with performing synthesis of ACNT; Vambola Kisand and Urmas Joost for analysing and measuring XPS spectra; Kaija Põhako for measuring and analysing FT-IR spectra and help with advises about nanotubes functionalization; Nadja Aleksejeva and Kaido Tammeveski for collaboration in nitrogen doped carbon nanotubes electrochemical measurements; Madis Lobjakas for help with electronics.

Also I would like to thank Rünno Lõhmus, Sergei Vlassov, Fredrik Punga, Tanel Tätte.

I thank my family and friends for support, understanding and believe in me.

Work was supported by Estonian Science Foundation grant 8420 and the Estonian Nanotechnology Competence Centre (grant EU29996).



## **PUBLICATIONS**

# CURRICULUM VITAE

## General data

Name and surname: Jevgeni Shulga  
Date and place of birth: 29.04.1982, Sillamäe, Estonia  
Citizenship: Estonia  
Telephone: +372 55943419

## Education

1989–2000 Sillamäe Kesk Gymnasium  
2000–2005 University of Tartu, baccalaureus scientiarum (BSc),  
material science  
2005–2007 University of Tartu, magister scientiarum (MSc),  
material science  
2007–2012 University of Tartu, PhD student, material science

## Professional employment

2003–2005 Laborant, IPUT, Laboratory of Physics of  
Nanostructures  
2005–... Engineer, IPUT, Laboratory of Physics of  
Nanostructures

## Professional Development

CFN Summer School 2006 on “Molecular Nanostructures” (Bad Herrenalb, Germany, September 03–07)

## Awards

2006 University of Tartu, Institute of Physics, student award “Preparation of oxide microstructures”

# ELULOOKIRJELDUS

## Üldandmed

Ees- ja perekonnanimi: Jevgeni Šulga  
Sünniaeg ja koht: 29.04.1982, Sillamäe, Eesti  
Kodakonsus: Eesti  
Kontaktandmed: Tartu Ülikooli Füüsika Instituut, Riia 142, 51014,  
Tartu, Eesti  
Telefon: +372 55943419

## Haridus

1989–2000	Sillamäe Keskkool
2000–2005	Tartu Ülikool, BSc, materjaliteadus
2005–2007	Tartu Ülikool, MSc, materjaliteadus
2007–2012	Tartu Ülikool, doktorant, materjaliteadus

## Teenistuskäik

2003–2005	Füüsika Instituut, laborant
2005–...	Füüsika Instituut, inseneer

## Erialane enesetäendus

CFN Suvekool 2006 “Molkulaarsed nanostruktuurid” (Bad Herrenalb, Saksa-  
maa, September 03–07)

## Preemiad

2006 TÜ Füüsika Instituudi üliõpilasstipendium

# DISSERTATIONES SCIENTIAE MATERIALIS

## UNIVERSITATIS TARTUENSIS

1. **Martin Järvekülg.** Tubular microstructures by Hf-, Zr- and Ti-butoxide gel sheet rolling. Tartu, 2011, 112 p.
2. **Sergei Vlassov.** Investigation of nanoscale interactions and mechanical properties of nanostructures using quartz tuning fork based real-time measurements. Tartu, 2011, 171 p.
3. **Margus Kodu.** Pulsed Laser Deposition of Magnesium Oxide and Barium Ternary Oxides for Plasma Display Protective Layers. Tartu, 2011, 89 p.
4. **Rainer Pärna.** Surface studies of some oxide films. Tartu, 2011, 129 p.